

Dear Editor,

We are thankful for bringing the review of this study this far. All this work has improved the manuscript significantly and we highly appreciate it. We have addressed all the points by the referees. Please see below the list of addressed comments.

With kind regards,

Andreia Plaza-Faverola

Ref 1:

line 423 (page 14): please delete "thus" from the sentence. It seems out of place.

A: corrected.

line 445 (page 15) should 'maximums' not be 'maxima'?

A: isn't "Maximums" becoming the new standard plural of "maximum" 😊. "Maxima" was commonly used in the past.

Ref 2:

I congratulate with the authors for the work done. This is a first important step to assess the relevance of tectonic stress propagation in the sedimentary cover of continental margins in controlling fluid migration in the long term. I acknowledge the work done to improve the manuscript according to the reviews received in the first round. I add below a few overall minor remarks and suggestions addressing some aspects not covered before.

Line 219. Earthquakes focal mechanisms. In the introduction (line 94), you state that earthquakes focal mechanisms provide poorly constrained stress vectors. However, in following analysis the focal mechanisms are used as a robust evidence of the stress field, so that they can be used to validate the results of the model. I wonder why the rather clear evidence from focal mechanisms was not properly used. Perhaps the initial statement in the introduction should be smoothed?

A: Thank you for identifying this. We have changed the sentence in the introduction for coherency.

Line 232 and following text. One important aspect of your analysis, somehow not properly valued in the paper (although you address it in the discussion), is the role of compaction disequilibrium in the sedimentary column as a factor of weakening the strength of the sediments and therefore allowing the rupture to propagate upwards. I have a few arguments here that could be incorporated in the text with the purpose to give even more emphasis to the role of undercompaction:

You state rather vaguely here that the sedimentary column below the Vestnesa Ridge is not expected to be highly consolidated. I would not use the term 'highly consolidated'. Sediments are either normal- or over- or under- consolidated. Over consolidation results from the maximum stress experienced by the sediment being higher than the present stress. This occurs only in the case of subaqueous erosion (tectonic or sedimentary), or exhumation of a marine sedimentary sequence, which is not your case. In a sedimentary sequence experiencing continuous sedimentation, like the Vestnesa sediment drift, you either have normal consolidation (if excess pore water induced by sedimentation can dissipate without building overpressure) or underconsolidation (in the case you have a rapidly building total stress in consequence of rapid sedimentation, or increase in the volume of the pore fluids by, in your case, volumetric expansion of methane).

In this case your pore pressure may increase above hydrostatic, with decreasing effective stress (decreasing strength), to the point of reaching the total stress. Above this limit you may have hydrofracturing and sediment inflation. (I think this is the process you describe citing “ the minimum effective stress is negative in Line 428. So hydrofracturing in the sedimentary column may be induced independently, without the crustal stress contribution, by a combination of increasing sedimentary load and increasing pore fluid volume. Of course in your case you are adding another factor that is the propagation of the crustal stress into the sedimentary column. In your case this contribution of tensile stress is towards a decrease of the total stress on the grains in favor of underconsolidation. I see you refer to this in Line 425. Later in the discussion you report a more important details, like the sedimentation rate. It would be important to know also the lithology (sampled or inferred). This is because it is generally assumed that in low permeability sediments (clay-rich formations), a sedimentation rate of 1 mm a-1 is enough to produce a situation of underconsolidation alone (Rubey & Hubbert 1959; Fertl 1976). You are not too far from this value below the crest of the ridge. I would rephrase your sentence in Lines 320-322 not I the sense of a stress build up, but rather a strength decrease due to compaction disequilibrium.

I am mentioning this because I think you should make even more clear in your discussion, the role of the consolidation state in the Vestnesa Ridge sedimentary sequence, saying that pore fluid overpressure (decreasing strength) may results from rapid sedimentation rate and fluid volume increase (gas expansion), below the crest of the ridge (the depocentre). The decreased effective stress in this area is a good explanation of the reason why you find the gas expulsion features and the faults here.

RUBEY, W.W. & HUBBERT, M.K. 1959. Role of fluid pressure in mechanics of overthrust faulting: II. Overthrust belt in geosynclinal area of western Wyoming in light of fluid-pressure hypothesis. Geological Society of America Bulletin, 70, 167–206

FERTL, W.H. 1976. Abnormal Formation Pressures. Implications to Exploration, Drilling, and Production of Oil and Gas Resources. Developments in Petroleum Science, 2. Elsevier, Amsterdam.

A: Thanks again for raising this issue. This is a complex aspect of the system. The degree of consolidation of the sediment in the region remains uninvestigated. We have modified the sentence in line 232 to indicate this instead of speculating about the compaction.

In lines 320-330 we have included information about the lithology reported from gravity cores. We have also modified our statement to hint on the potential effect of under compaction (due to high sed rates and sediment grain size but also due to tectonic forcing) on effective stress. However, after revising the papers suggested by the referee and other papers studying consolidation of deep marine sediments (e.g., Buchan and Smith 1999), we realized that the upper sediments on Vestnesa may be under consolidated due to fast sedimentation and increase in pore fluid volume (as the referee points out) but on the other hand, the presence of authigenic carbonate and gas hydrates may favor over consolidation (or shift the consolidation curve on the opposite direction) and somehow compensate the abnormal effect on the compaction curve. This is a topic to be investigated in more depth, we hope that future experiments in the region will help in this matter. Nevertheless, the conditions for undercompaction and weakening of the sediment would be given along the entire ridge. Actually the highest sedimentation rate is towards the western segment. Hence, a decrease in the effective stress due to horizontal forcing in a tensile regime is still the best explanation for the focused seepage on the eastern segment.

We added emphasis with one sentence in the conclusion, to the importance of the effect of overpressure on decreasing the horizontal stress and favoring fracturing and dilation of existing faults particularly under the tensile stress regime at the eastern part of the ridge.

Line 419. The role of gas hydrates in making the faults and fractures less permeable to fluid migration is very important. I suggest to cite and use the results of the paper:

Madrussani et al., 2009. Gas hydrates, free gas distribution and fault pattern on the west Svalbard continental margin. GJI. doi: 10.1111/j.1365-246X.2009.04425.x

Where the authors provide geophysical evidence (Vp, Vs and attenuation) of the role of gas hydrates in decreasing the permeability of the faults and driving lateral gas migration below the base of the GHSZ.

A: Great suggestion, thanks. We have included a reference to this work, we evoke their models as example of other areas where fluid dynamics at the base of the GHSZ due to sealing of faults by hydrates result plausible.

Line 498. The meaning of bathymetry as a source of stress is, at least to me, a bit unclear. I understand you mean gravitational forces along a slope. Is it so? Is stress induced by bathymetry coded?

A: We changed to gravitational forcing. We are not aware of any documentation of the forcing by bathymetry across the Svalbard margin. We hope this will be included in future models.

Minors:

Line 243 replace "gentle" with "small"

A: corrected

Line 288. Replace "understood" with "considered"

A: corrected

Line 312. replace "nearby" with "focusing around"

A: corrected

Line 355. I would delete the sentence "All the conditions are given for sustaining seepage along the entire ridge" as I find it unnecessary.

A: suggestion accepted.

1 **CORRELATION BETWEEN TECTONIC STRESS REGIMES AND METHANE SEEPAGE ON THE**
2 **WEST-SVALBARD MARGIN**

3
4 A. Plaza-Faverola¹ and M. Keiding²

5 ¹ CAGE-Centre for Arctic Gas Hydrate, Environment, and Climate; Department of Geosciences, UiT The Arctic
6 University of Norway, N-9037 Tromsø, Norway

7 ² Geological Survey of Norway (NGU), P.O. Box 6315 Torgarden, 7491 Trondheim, Norway

8 *Correspondence to:* Andreia Plaza-Faverola (Andreia.a.faverola@uit.no)

9 **Abstract.** Methane seepage occurs across the west-Svalbard margin at water depths ranging from < 300 m,
10 landward from the shelf break, to > 1000 m in regions just a few kilometres away from the mid-ocean ridges in
11 the Fram Strait. The mechanisms controlling seepage remain elusive. The Vestnesa sedimentary ridge, located on
12 oceanic crust at 1000-1700 m water depth, hosts a perennial gas hydrate and associated free gas system. The
13 restricted occurrence of acoustic flares to the eastern segment of the sedimentary ridge, despite the presence of
14 pockmarks along the entire ridge, indicates a spatial variation in seepage activity. This variation coincides with a
15 change in the faulting pattern as well as in the characteristics of fluid flow features. Due to the position of the
16 Vestnesa ridge with respect to the Molloy and Knipovich mid-ocean ridges, it has been suggested that seepage
17 along the ridge has a tectonic control. We modelled the tectonic stress regime due to oblique spreading along the
18 Molloy and Knipovich ridges to investigate whether spatial variations in the tectonic regime along the Vestnesa
19 Ridge are plausible. The model predicts a zone of tensile stress that extends northward from the Knipovich Ridge
20 and encompasses the zone of acoustic flares on the eastern Vestnesa Ridge. In this zone the orientation of the
21 maximum principal stress is parallel to pre-existing faults. The model predicts a strike-slip stress regime in
22 regions with pockmarks where acoustic flares have not been documented. If a certain degree of coupling is
23 assumed between deep crustal and near-surface deformation, it is possible that ridge push forces have influenced
24 seepage activity in the region by interacting with the pore-pressure regime at the base of the gas hydrate stability
25 zone. More abundant seepage on the eastern Vestnesa Ridge at present may be facilitated by dilation of faults and
26 fractures favourably oriented with respect to the stress field. A modified state of stress in the past, for instance
27 due to more significant glacial stress, may have explained a vigorous seepage activity along the entire Vestnesa
28 Ridge. The contribution of other mechanisms to the state of stress (i.e., sedimentary loading and lithospheric
29 flexure) remain to be investigated. Our study provides a first order assessment of how tectonic stresses may be
30 influencing the kinematics of near-surface faults and associated seepage activity offshore the west-Svalbard
31 margin.

32

33

34 **1. Introduction**

35 Hundreds of gigatonnes of carbon are stored as gas hydrates and shallow gas reservoirs in continental margins
36 (e.g., Hunter et al., 2013). The release of these carbons over geological time, a phenomenon known as methane
37 seepage, is an important contribution to the global carbon cycle. Understanding and quantifying seepage has
38 important implications for ocean acidification, deep-sea ecology and global climate. Periods of massive methane
39 release from gas hydrate systems (e.g., Dickens, 2011) or from large volcanic basins like that in the mid-
40 Norwegian margin (e.g., Svensen et al., 2004) have been linked to global warming events such as the Palaeocene-
41 Eocene thermal maximum. In addition, methane seepage and near-seafloor gas migration have implications for
42 geohazards, since pore-fluid pressure destabilization is one factor associated with the triggering of submarine
43 land-slides (e.g., DeVore and Sawyer, 2016; Urlaub et al., 2015). It is well known that seepage at continental
44 margins has been occurring episodically for millions of years (e.g., Judd and Hovland, 2009), but there is a poor
45 understanding of what forces it.

46

47 Present day seepage is identified as acoustic flares in the water column commonly originating at seafloor
48 depressions (e.g., Chand et al., 2012; Salomatin and Yusupov, 2011; Skarke et al., 2014; Smith et al.,
49 2014; Westbrook et al., 2009), while authigenic carbonate mounds are used as indicators of longer-term seepage
50 activity (e.g., Judd and Hovland, 2009). Seepage at the theoretical upstream termination of the gas hydrate
51 stability zone (GHSZ) (i.e., coinciding with the shelf edge) at different continental margins, has been explained
52 by temperature driven gas-hydrate dissociation (e.g., Skarke et al., 2014; Westbrook et al., 2009). On formerly
53 glaciated regions off Svalbard and the Barents Sea, active seepage has been explained by gas hydrate dissociation
54 either due to pressure changes resulting from the retreat of the ice-sheet (e.g., Portnov et al., 2016; Andreassen et
55 al., 2017) or to post-glacial uplift (Wallmann et al., 2018).

56

57 Across the west-Svalbard margin, active seepage extends beyond the shelf break and the region formerly covered
58 by ice. As a matter of fact, active seepage sites have been identified from inside Isfjorden (Roy et al., 2014) to
59 water depths of ~1200 m (Smith et al., 2014) where the Vestnesa Ridge hosts a perennially stable gas hydrate
60 system > 50 km seaward from the ice-sheet grounding line. The Vestnesa Ridge is a NW-SE oriented contourite
61 deposit located between the northward termination of the Knipovich Ridge and the eastern flank of the Molloy
62 spreading ridge in the Fram Strait (Fig. 1). Seafloor pockmarks along the Vestnesa Ridge, first documented by

63 Vogt et al., (1994), exist along the entire ridge. However, acoustic flares have been observed to originate
64 exclusively at large pockmarks located on the eastern part of the sedimentary ridge (Fig. 2, 3). A clear increase in
65 seepage activity towards the easternmost part of the ridge is thus evident from multiple year's water-column
66 acoustic surveys (Petersen et al., 2010;Bünz et al., 2012;Plaza-Faverola et al., 2017;Smith et al., 2014). In this
67 paper, we use the terminology “active” and “inactive” to differentiate between sites with and without documented
68 acoustic flares. Even though methane advection and methanogenesis are likely to be active processes along the
69 entire Vestnesa Ridge, the presence of inactive pockmarks adjacent to a zone of active seepage, raises the
70 question what controls temporal and spatial variations in seepage activity along the ridge?

71

72 Plaza-Faverola et al., (2015) documented seismic differences in the orientation and type of faulting along the
73 ridge and showed a link between the distribution of gas chimneys and faults. They hypothesised that seepage
74 activity may be explained by spatial variation in tectonic stress field across the margin (Plaza-Faverola et al.,
75 2015). However, the state of stress across Arctic passive margins has not been investigated. The total state of
76 stress at formerly glaciated continental margins can be the result of diverse factors including bathymetry and
77 subsurface density contrasts, subsidence due to glacial or sedimentary loading and lithospheric cooling, in
78 addition to ridge-push forces (Fejerskov and Lindholm, 2000;Lindholm et al., 2000;Olesen et al., 2013;Stein et
79 al., 1989;Grunnaleite et al., 2009).

80

81 The interaction between the above mentioned factors renders modelling of the total state of stress a complex
82 problem that has not yet been tackled. In this study, we focus exclusively on the potential contribution of oblique
83 spreading at the Molloy and the Knipovich ridges to the total state of stress along the Vestnesa Ridge and do a
84 qualitative analysis of how stress generated by mid-ocean ridge spreading may influence near-surface faulting
85 and associated seepage activity. The study of the effect of ridge push forces on near-surface deformation across
86 the west-Svalbard margin contributes to the current debate about neo-tectonism and stress field variations across
87 passive margins (Olesen et al., 2013;Salomon et al., 2015). It also has implications for understanding the
88 mechanisms that control seepage at continental margins globally. Splay-faults are found to drive fluid migration
89 at subduction margins and to sustain shallow gas accumulations and seepage (e.g., Plaza-Faverola et al.,
90 2016;Minshull and White, 1989;Moore and Vrolijk, 1992;Crutchley et al., 2013), and the relationship between
91 fault kinematics and fluid migration has been documented specially at accretionary margins where earthquake-
92 induced seafloor seepage has been observed (e.g., Geersen et al., 2016). So far, the information about the present
93 day stress regime in the Fram Strait has been limited to large scale lithospheric density models (Schiffer et al.,

94 2018) ~~and a limited number of stress vectors from earthquake focal mechanisms from the mid-ocean ridge axes~~
95 a number of stress vectors from earthquake focal mechanisms along the mid-Atlantic plate boundary (Heidbach
96 et al., 2016). Our study provides a first order assessment of how stresses from slow spreading mid-ocean ridges
97 may be influencing the kinematics of near-surface faults and associated seepage activity in an Arctic passive
98 margin.

99

100 **2. Structural and stratigraphic setting**

101 In the Fram Strait, sedimentary basins are within tens of kilometres from ultra-slow spreading Arctic mid-ocean
102 ridges (Fig. 1). The opening of the Fram Strait was initiated 33 Ma ago and evolved as a result of slow spreading
103 of the Molloy and Knipovich Ridges (Engen et al., 2008). An important transpressional event deformed the
104 sedimentary sequences off western Svalbard, resulting in folds and thrustbelts, during the Paleocene-Eocene
105 dextral movement of Spitsbergen with respect to Greenland. Transpression stopped in the early Oligocene when
106 the tectonic regime became dominated by extension (Myhre and Eldholm, 1988). The circulation of deep water
107 masses through the Fram Strait started during the Miocene, ca. 17-10 Ma ago (Jakobsson et al., 2007; Ehlers and
108 Jokat, 2009), and established the environmental conditions for the evolution of bottom current-driven
109 sedimentary drifts (Eiken and Hinz, 1993; Johnson et al., 2015). It has been suggested that the opening of the
110 northern Norwegian–Greenland Sea was initiated by the northward propagation of the Knipovich ridge into the
111 ancient Spitsbergen Shear Zone (Crane et al., 1991).

112

113 The continental crust beneath the western coast of Svalbard thins towards the Hornsund Fault zone indicating
114 extension following the opening of the Greenland Sea (Faleide et al., 1991). Late Miocene and Pliocene
115 sedimentation, driven by bottom currents, resulted in the formation of the ca. 100 km long Vestnesa Ridge
116 between the shelf break off west-Svalbard and oceanic crust highs at the eastern flank of the Molloy mid-ocean
117 ridge (Eiken and Hinz, 1993; Vogt et al., 1994). The sedimentary ridge is oriented parallel to the Molloy
118 Transform Fault and its crest experiences a change in morphology from narrow on the eastern segment to broader
119 on the western Vestnesa Ridge segment (Fig. 2). The exact location of the continental-ocean transition remains
120 uncertain (Eldholm et al., 1987) but it is inferred to be nearby the transition from the eastern to the western
121 segments (Engen et al., 2008).

122

123 The total sedimentary thickness along the Vestnesa Ridge remains unconstrained. Based on one available
124 regional seismic profile it can be inferred that the ridge is > 5 km thick in places (Eiken and Hinz, 1993). It has

125 been divided into three main stratigraphic units (Eiken and Hinz, 1993;Hustoft, 2009): the deepest sequence,
126 YP1, consists of synrift and post-rift sediments deposited directly on oceanic crust; YP2 consists of contourites;
127 and YP3, corresponding to the onset of Pleistocene glaciations (ca. 2.7 Ma ago) (Mattingsdal et al., 2014), is
128 dominated by glaciomarine contourites and a mix with turbidites in regions close to the shelf break. The effect of
129 ice-sheet dynamics on the west-Svalbard margin (Patton et al., 2016;Knies et al., 2009) has influenced the
130 stratigraphy, and most likely the morphology, of the Vestnesa Ridge and adjacent sedimentary basins. In this
131 Arctic region, glaciations are believed to have started even earlier than 5 Ma ago. The local intensification of
132 glaciations is inferred to have started ca. 2.7 Ma ago (e.g., Faleide et al., 1996;Mattingsdal et al., 2014). Strong
133 climatic fluctuations characterized by intercalating colder, intense glaciations with warmer and longer
134 interglacials, dominated the last ca. 1 Ma. (e.g., Jansen et al., 1990;Jansen and Sjøholm, 1991).

135

136 **3. Seismic data**

137 The description of faults and fluid flow related features along the Vestnesa Ridge is documented by several
138 authors (Bünz et al., 2012;Hustoft, 2009;Petersen et al., 2010;Plaza-Faverola et al., 2015;Plaza-Faverola et al.,
139 2017). Two-3D high resolution seismic data sets acquired on the western and the eastern Vestnesa Ridge
140 respectively (Fig. 2), and one 2D seismic line acquired along the entire Vestnesa Ridge extent have been
141 particularly useful in the description of the structures along the ridge (Fig. 2). These data have been previously
142 used for the investigation of the bottom simulating reflection dynamics (i.e., the seismic indicator of the base of
143 the gas hydrate stability zone) (Plaza-Faverola et al., 2017) and documentation of gas chimneys and faults in the
144 region (Petersen et al., 2010;Plaza-Faverola et al., 2015;Bünz et al., 2012). The 3D seismic data were acquired on
145 board R/V Helmer Hanssen using the high resolution P-Cable system (Planke et al., 2009). The 2D lines were
146 also collected connecting 4 streamers from the P-Cable system for 2D acquisition. Final lateral resolution of the
147 3D data sets is given by a bin size of $6.25 \times 6.25 \text{ m}^2$ and the vertical resolution is $> 3 \text{ m}$ with a dominant frequency
148 of 130 Hz. Details about acquisition and processing can be found in Petersen et al., 2010 and Plaza-Faverola et
149 al., 2015. For the 2D survey the dominant frequency was $\sim 80 \text{ Hz}$ resulting in a vertical resolution $> 4.5 \text{ m}$
150 (assumed as $\lambda/4$ with an acoustic velocity in water of 1469 m/s given by CTD data; Plaza-Faverola et al., 2017).

151

152 **4. The modelling approach**

153 The modelling carried out in this study deals exclusively with tectonic stress due to ridge push. We use the
154 approach by Keiding et al. (2009) based on the analytical solutions derived by Okada (1985), to model the plate
155 motion and tectonic stress field due to spreading along the Molloy and Knipovich Ridges.

156

157 The Okada model and our derivation of the stress field from it is described in more detail in appendix A. The
158 Molloy and Knipovich Ridges are modelled as rectangular planes with opening and transform motion in a flat
159 Earth model with elastic, homogeneous, isotropic rheology (Fig. A1 in appendix). Each rectangular plane is
160 defined by ten model parameters used to approximate the location, geometry and deformation of the spreading
161 ridges (Okada, 1985; see supplement Table 1). The locations of the two spreading ridges were constrained from
162 bathymetry maps (Fig. 1). The two spreading ridges are assumed to have continuous, symmetric deformation
163 below the brittle-ductile transition, with a half spreading rate of 7 mm/yr and a spreading direction of N125°E,
164 according to recent plate motion models (DeMets et al., 2010). Because the spreading direction is not
165 perpendicular to the trends of the spreading ridges, this results in both opening and right-lateral motion; that is,
166 oblique spreading on the Molloy and Knipovich Ridges. The Molloy Transform Fault, which connects the two
167 spreading ridges, trends N133°E, thus a spreading direction of N125°E implies extension across the transform
168 zone. We use a depth of 10 km for the brittle-ductile transition and 900 km for the lower boundary of the
169 deforming planes, to avoid boundary effects. For the elastic rheology, we assume typical crustal values of
170 Poisson's ratio = 0.25 and shear modulus = 30 GPa (Turcotte and Schubert, 2002). We perform sensitivity tests
171 for realistic variations in 1) model geometry, 2) spreading direction, 3) depth of the brittle-ductile transition, and
172 4) Poisson's ratio (Supplementary material). Variations in shear modulus, e.g. reflecting differences in elastic
173 parameters of crust and sediments, would not influence the results, because we do not consider the magnitude of
174 the stresses.

175

176 Asymmetric spreading has been postulated for the Knipovich Ridge based on heat flow data (Crane et al., 1991),
177 and for other ultraslow spreading ridges based on magnetic data (e.g., Gaina et al., 2015). However, the evidence
178 for asymmetry along the Knipovich Ridge remains inconclusive and debatable in terms, for example, of the
179 relative speeds suggested for the North American (faster) and the Eurasian (slower) plates (Crane et al.,
180 1991; Morgan, 1981; Vogt et al., 1994). This reflects that the currently available magnetic data from the west-
181 Svalbard margin is not of a quality that allows an assessment of possible asymmetry of the spreading in the Fram
182 Strait (Nasuti and Olesen, 2014). Symmetry is thus conveniently assumed for the purpose of the present study.

183

184 We focus on the stress field in the upper part of the crust (where the GHSZ is) and characterise the stress regime
185 based on the relationship between the horizontal and vertical stresses. We refer to the stresses as σ_v (vertical
186 stress), σ_H (maximum horizontal stress) and σ_h (minimum horizontal stress), where compressive stress is positive

187 (Zoback and Zoback, 2002). A tensile stress regime ($\sigma_v > \sigma_H > \sigma_h$) favours the opening of steep faults that can
188 provide pathways for fluids. Favourable orientation of stresses with respect to existing faults and/or pore fluid
189 pressures increasing beyond hydrostatic pressures are additional conditions for leading to opening for fluids
190 under strike-slip ($\sigma_H > \sigma_v > \sigma_h$) and compressive ($\sigma_H > \sigma_h > \sigma_v$) regimes (e.g., Grauls and Baleix, 1994).

191

192 **5. Results**

193 **5.1 Predicted type and orientation of stress fields due to oblique spreading at the Molloy and the Knipovich** 194 **ridges**

195 The model predicts zones of tensile stress near the spreading ridges, and strike-slip at larger distances from the
196 ridges. An unexpected pattern of tensile stress arises from the northward termination and the southward
197 termination of the Knipovich and Molloy ridges respectively (Fig. 3). The zone of tensile stress that extends
198 northward from the Knipovich Ridge, encompasses the eastern part of the Vestnesa Ridge. The western Vestnesa
199 Ridge, on the other hand, lies entirely in a zone of strike-slip stress (Fig. 3). The sensitivity tests show that the
200 tensile stress zone is a robust feature of the model, that is, variations in the parameters result in a change of the
201 extent and shape of the tensile zone but the zone remains in place (Supplementary material). It appears that the
202 tensile zone is a result of the interference of the stress from the two spreading ridges. To illustrate this, we ran the
203 model for the Molloy Ridge and the Knipovich Ridge independently. In the model with Knipovich Ridge alone, a
204 large tensile zone extends northeast from the ridge's northern end, covering only the easternmost corner of
205 Vestnesa Ridge (Fig. 4). Under the influence of the strike-slip field from the Molloy Ridge, this zone is deflected
206 and split into two lobes, of which one extends to the eastern Vestnesa Ridge segment.

207

208 To investigate the geometric relationship between the predicted stress field and mapped faults, we calculated the
209 orientations of maximum compressive horizontal stress (Lund and Townend, 2007). The maximum horizontal
210 stresses (σ_H) approximately align with the spreading axes within the tensile regime and are perpendicular to the
211 axes within the strike-slip regime (Fig. 3). Spreading along the Molloy ridge causes NW-SE orientation of the
212 maximum compressive stress along most of the Vestnesa Ridge, except for the eastern segment where the
213 influence of the Knipovich Ridge results in a rotation of the stress towards E-W (Fig. 3).

214

215 The simplifying assumptions involved in our model imply that the calculated stresses in the upper crust are
216 unconstrained to a certain degree. However, the predicted stress directions are in general agreement with other
217 models of plate tectonic forces (e.g., Gölke and Coblentz, 1996; Naliboff et al., 2012). In addition, Árnadóttir et

218 al. (2009) demonstrated that the deformation field from the complex plate boundary in Iceland could be modelled
219 using Okada's models. More importantly, a comparison of the predicted strike-slip and tensile stress fields from
220 plate spreading and observed earthquake focal mechanisms shows an excellent agreement, both with regards to
221 stress regime and orientation of maximum compressive stress. The earthquake focal mechanisms are mostly
222 normal along the spreading ridges and strike-slip along the transform faults, and the focal mechanism pressure
223 axes align nicely with the predicted directions of maximum compressive stress (Fig. 3). The good agreement
224 between Okada's model and other modelling approaches as well as between the resulting stresses and focal
225 mechanisms in the area indicates that the model, despite the simplicity of its assumptions, provides a correct first
226 order prediction of orientation and type of the stress field in the upper crust (other possible sources of stress in the
227 region will be discussed in more detail in section 6.1). It remains an open question to which degree the crustal
228 stresses are transferred to the sedimentary successions of the Vestnesa Ridge. For compacted stratigraphic
229 formations in the Norwegian Sea, a comparison of shallow in-situ stress measurements and deeper observations
230 from earthquake focal mechanisms indicates that the stress field is homogeneous in direction over a large depth
231 range (Fejerskov and Lindholm, 2000). For an overburden constituted of Quaternary sediments, though, the stress
232 coupling between the crust and the near-surface depends on the shear strength of the sediments. The upper 200 m
233 of hemipelagic sediment along the Vestnesa Ridge are relatively young (< 2 Ma) and ~~not expected to be highly~~
234 ~~consolidated~~the degree of sediment consolidation remains uninvestigated. However, the fact that a large number
235 of faults extend several hundred meters through the sediments suggests that compaction of the sediments has
236 been large enough to build up some amount of shear strength. Geotechnical studies from different continental
237 margins indicate that deep marine sediments can experience high compressibility due to the homogeneity in the
238 grain structure (i.e., large areas made of a single type of sediment), providing favourable conditions for shear
239 failure (Urlaub et al., 2015; DeVore and Sawyer, 2016). Therefore, we consider possible that the upper
240 sedimentary column along the Vestnesa Ridge has been deformed by tectonic stress.

241

242 **5.2 Distribution of faults and seepage activity along the Vestnesa Ridge with respect to modelled tectonic** 243 **stress**

244 High-resolution 3D seismic data collected on the eastern Vestnesa Ridge revealed sub-seabed NW-SE oriented,
245 near-vertical faults with a small normal throw (< 10 m; Fig. 5). In this part of the Vestnesa Ridge, gas chimneys
246 and seafloor pockmarks are ca. 500 m in diameter. On structural maps extracted along surfaces within the GHSZ
247 gas chimneys project over fault planes or at the intersection between fractures (Fig. 2, 3c). A set of N-S to NNE-
248 SSE trending faults outcrop at the seafloor at a narrow zone between the Vestnesa Ridge and the northern

249 termination of the Knipovich Ridge (Fig 1, 2). These faults have been suggested to indicate ongoing northward
250 propagation of the Knipovich rift system (Crane et al., 2001;Vanneste et al., 2005). The NW-SE oriented sub-
251 seabed faults and fractures at the crest of the Vestensa Ridge could be genetically associated with these
252 outcropping faults (Plaza-Faverola et al., 2015; Fig. 2).

253

254 Most of the outcropping N-S to NNE-SSE oriented faults north of the Knipovich Ridge and the sub-seafloor NW-
255 SE oriented faults on the eastern Vestnesa Ridge are located within the zone of modelled tensile regime that
256 extends northward from the Knipovich Ridge (Fig. 3). The orientation of σ_H rotates from being perpendicular to
257 the Molloy ridge nearby sub-seafloor faults at the eastern Vestensa Ridge, to be more perpendicular to the
258 Knipovich Ridge in places within the tensile zone (Fig. 3). Interestingly, documented acoustic flares along the
259 Vestensa Ridge are also located within the zone of modelled tensile stress regime (Fig. 3). The match between the
260 extent of the modelled tensile regime and the active region of pockmarks is not exact; pockmarks with acoustic
261 flares exist a few kilometres westward from the termination of the tensile zone (Fig. 3). However, the agreement
262 is striking from a regional point of view. Some of the outcropping faults north of the Knipovich Ridge and south
263 of the Molloy transform fault appear located outside the modelled tensile zone (Fig. 3; Fig. S1-S4 in the
264 supplement). Inactive pockmarks (i.e., no acoustic flares have been observed during several visits to the area) are
265 visible on high resolution bathymetry maps over these faulted regions (Dumke et al., 2016;Hustoft, 2009;Johnson
266 et al., 2015;Waghorn et al., 2018).

267

268 In a similar high-resolution 3D seismic data set from the western Vestnesa Ridge the faults have different
269 characteristics compared to those of the eastern segment. In this part of the ridge gas chimneys are narrower,
270 buried pockmarks are stacked more vertically than the chimneys towards the east and it is possible to recognise
271 more faults reaching the present-day seafloor (Plaza-Faverola et al., 2015). Fault segments are more randomly
272 oriented with a tendency for WNW-ESE and E-W orientations (Fig. 2). These structures coincide with a
273 modelled strike-slip stress regime with σ_H oriented nearly perpendicular to the Molloy Ridge (Fig. 3).

274

275 **6. Discussion**

276 The striking coincidence between the spatial variation in modelled stress regimes and the pattern of faulting and
277 seepage activity along the Vestnesa Ridge leads to the discussion whether tectonic stresses resulting from plate
278 spreading at the Molloy and the Knipovich ridges have the potential to influence near-surface deformation and
279 fluid dynamics in the study area. We discuss first the modelling results in the context of the total state of stress

280 across passive margins and to which extent regional stresses can influence near-surface deformation. Assuming
281 that tectonic stress can potentially influence near-surface deformation, we discuss then the effect that the
282 modelled stress fields would have on pre-existing faults and associated fluid migration. Finally, we propose a
283 model for explaining seepage evolution along the Vestnesa Ridge coupled to stress field variations. We close the
284 discussion with a note on the implications of the present study for understanding near-surface fluid dynamics
285 across passive margins globally.

286

287 **6.1 Modelled stress in the context of the state of stress along the Vestnesa Ridge**

288 In this study we focused exclusively on modelling the type and orientation of stresses potentially generated by
289 spreading at the Molloy and Knipovich ridges. Other sources of stress have been so far disregarded. Hence, the
290 modelled stress field documented in this study cannot be considered as a representation of the total stress field in
291 the region. Modelling studies from Atlantic-type passive margins, suggest that from all the possible sources of
292 stress across passive margins (i.e., sediment loading, glacial flexure, spatial density contrasts, and ridge push as
293 well as basal drag forces) sediment loading (assuming elastic deformation) appears to be the mechanism with the
294 potential of generating the largest magnitudes of stresses across passive margins (Stein et al., 1989; Turcotte et al.,
295 1977). However, stress information derived from seismological and in-situ data (Fjeldskaar and Amantov,
296 2018; Grunnaleite et al., 2009; Lindholm et al., 2000; Olesen et al., 2013) and paleo-stress field analyses based on
297 dip and azimuth of fault planes (Salomon et al., 2015) point towards a dominant effect of ridge push forces on the
298 state of stress across passive continental margins. Given the proximity of the Vestnesa Ridge to the Molloy and
299 the Knipovich ridges (Fig. 1), we argue that tectonic stress from spreading can be an important factor, perhaps
300 even a dominant factor, controlling near-surface deformation along the Vestnesa Ridge.

301

302 The contemporary stress field across the west-Svalbard passive margin is presumably the result of an interaction
303 between large-scale tectonic stress mechanisms (i.e., ridge push, basal drag) overprinted by regional (i.e., density
304 contrasts, glacial related flexure, sediment loading) and local mechanisms (e.g., topography, pore-fluid pressure
305 variations, faulting). In the concrete case of the Vestnesa Ridge, a change in the faulting pattern, the distribution
306 of shallow gas and gas hydrates, as well as differences in the topographic characteristics of the ridge crest (Fig. 2,
307 5), are all factors likely to induce local changes in the degree of compaction and in near-surface stress. We
308 discuss in the following sections how local stress-generating mechanisms may interact with tectonic forcing to
309 control fluid dynamics and seepage.

310

311 The Vestnesa sedimentary Ridge sits over relatively young oceanic crust, < 19 Ma old (Eiken and Hinz,
312 1993;Hustoft, 2009). The oceanic-continental transition is not well constrained but its inferred location crosses
313 the Vestnesa Ridge at its easternmost end (Engen et al., 2008;Hustoft, 2009). This is a zone prone to flexural
314 subsidence due to cooling during the evolution of the margin and the oceanic crust may have experienced syn-
315 sedimentary subsidence focused around the oceanic-continental transition, as suggested for Atlantic passive
316 margins (Turcotte et al., 1977). However, syn-sedimentary subsidence would result in N-S oriented faults (i.e.,
317 reflecting the main direction of major rift systems during basin evolution) (Faleide et al., 1991;Faleide et al.,
318 1996). Although one N-S oriented fault outcrops in bathymetry data at the transition from the eastern to the
319 western Vestnesa Ridge segments (Fig. 5a), most of the sub-seabed faults and associated fluid migration features
320 in 3D seismic data are NW-SE to E-W oriented (Fig. 1, 2). ~~Similarly,~~

321
322 ~~†~~The weight of the contourite ridge over the oceanic crust may have generated additional stress on the Vestnesa
323 Ridge. ~~S~~However, sedimentation rates on the Vestnesa Ridge have been moderate, estimated to have fluctuated
324 between 0.1-0.6 mm/year since the onset of glaciations 2.7 Ma ago (Plaza-Faverola et al., 2017;Knies et al.,
325 2018;Mattingsdal et al., 2014). The lithology of the upper sediment along the ridge appears dominated by soft
326 fine-grained hemipelagic clayey silt with variable concentrations of ice-rafted debris (Szybor and Rasmussen,
327 2017a). Together, sedimentation rates and a high clay content would provide an ideal setting for
328 undercompaction due to increased pore fluid pressure (e.g., Fertl, 1976;Smith, 1999). High pore fluid pressure
329 would lead to a decrease in the effective stress and favour shearing (Grauls and Baleix, 1994). Whether these
330 sedimentation rates have allowed stress to build up through the upper strata faster than what it relaxes at the crust
331 (i.e., as expected for sedimentation rates larger than 1 mm/year (Stein et al., 1989)), as well as what has been the
332 role of gas hydrates and authigenic carbonate on the compaction history of the sediment –remains to be
333 investigated.

334
335 Glacial isostasy results in significant stresses associated with flexure of the lithosphere as the ice-sheet advances
336 or retreats. Present uplift rates are highest at the centre of the formerly glaciated region where the ice thickness
337 was at the maximum (Fjeldskaar and Amantov, 2018). Modelled present day uplift rates at the periphery of the
338 Barents sea ice-sheet ranges from 0 to -1 mm/year, depending on the ice-sheet model used in the calculation
339 (Auriac et al., 2016). This compares to an uplift rate of up to 9 mm/year at the centre of the ice sheet (Auriac et
340 al., 2016;Patton et al., 2016). Modelled glacial stresses induced by the Fennoscandian ice sheet on the mid-
341 Norwegian margin are close to zero at present day (Lund et al., 2009;Steffen et al., 2006). By analogy, present

342 day stress along the Vestnesa Ridge - located ~60 km from the shelf break - may be insignificant. It is likely that
343 glacial stresses as far off as the Vestnesa Ridge had a more significant effect in the past, as further discussed in
344 section 6.3 and 6.4.

345

346 Finally, ridge push forcing has the potential of being a dominant factor on the state of stress across the west-
347 Svalbard margin as observed for Norwegian margins (Fejerskov and Lindholm, 2000;Lindholm et al., 2000).
348 Specifically, the Vestnesa Ridge has the particularity that it is located within the expected range of maximum
349 influence of ridge push forces on the stress regime (Fejerskov and Lindholm, 2000) and that forces from two
350 spreading ridges influence it from different directions (i.e., the Molloy Ridge from the west and the Knipovich
351 Ridge from the south-east). The intriguing stress pattern appears to be caused by the interaction of the stress
352 generated by the two spreading ridges, as described above (section 5.1).

353

354 **6.2 Effect of the modelled stress fields on pre-existing faults and present day seepage**

355 Bearing in mind that several factors contribute to the total state of stress at different scales across passive margins
356 we assume that an influence on near-surface deformation by mid-ocean ridge stresses is plausible and discuss
357 their potential effect on seepage activity. Depending on the tectonic regime, the permeability through faults and
358 fractures may be enhanced or inhibited (e.g., Sibson, 1994;Hillis, 2001;Faulkner et al., 2010). Thus, spatial and
359 temporal variations in the tectonic stress regime may control the transient release of gas from the seafloor over
360 geological time as documented, for example, for CO₂ analogues in the Colorado Plateau (e.g., Jung et al., 2014).

361

362 A gas hydrate system is well developed and shallow gas accumulates at the base of the GHSZ along the entire
363 Vestnesa Ridge (Plaza-Faverola et al., 2017). Thermogenic gas accumulations at the base of the GHSZ (Fig. 5)
364 are structurally controlled (i.e., the gas migrates towards the crest of the sedimentary ridge) and together with
365 microbial methane this gas sustains present day seepage activity (Bünz et al., 2012;Plaza-Faverola et al.,
366 2017;Knies et al., 2018). However, seepage is focused and restricted. Some of the mechanisms commonly
367 invoked to explain seepage activity across passive margins include climate related gas hydrate dissociation, tidal
368 or seasonal sea-level changes, and pressure increases in shallow reservoirs due to fast sedimentation (e.g., Bünz
369 et al., 2003;Hustoft et al., 2010;Karstens et al., 2018;Riboulot et al., 2014;Skarke et al., 2014;Berndt et al.,
370 2014;Wallmann et al., 2018;Westbrook et al., 2009;Franek et al., 2017). While all of these mechanisms may
371 influence seepage systems as deep as the Vestnesa Ridge (> 1000 m deep; as discussed further in section 6.3)
372 they offer no explanation as to why seepage activity is more substantial within chimney sites proximal to or at

373 fault planes and why seepage is at a minimum or stopped elsewhere along the ridge (Fig. 2, 5). Overall, the
374 pattern of seepage activity along the Vestnesa Ridge is strikingly consistent with the modelled tectonic stress
375 field pattern. Acoustic flares have been documented to originate from < 10 m broad zones (Panieri et al., 2017)
376 within pockmarks located exclusively along faults. We suggest that these faults are favourably oriented with
377 respect to a tectonic σ_H (Fig. 2) and that opening of fault segments favourably oriented with respect to the stress
378 field is one controlling factor of present day seepage.

379

380 Present day seepage activity is less pronounced towards the western Vestnesa Ridge. Despite available gas
381 trapped at the base of the GHSZ (Fig. 5) the faults are generally less favourably oriented for tensile opening (i.e.,
382 NW-SE oriented σ_H) and are under a strike-slip regime (Fig. 2). The cluster of larger scale N-S to NNW-SSE
383 trending extensional faults that outcrop at the southern slope of the Vestnesa Ridge (Fig. 1, 2), also coincides
384 with the zone of predicted tensile stress (Fig. 3). However, the modelled maximum compressive stress in this area
385 is generally oblique to the fault planes, making these faults less open for gas. Interestingly, this is also a zone of
386 pockmarks where acoustic flares have not been observed (e.g., Johnson et al., 2015; Hustoft et al., 2009;
387 Vanneste et al., 2005). A set of N-S oriented structures south of the Molloy Transform Fault and a train of
388 pockmarks at the crest of a ridge west of the Knipovich Ridge axis are located under a strike-slip regime with N-
389 S oriented σ_H (Fig. 3). Although gas accumulations and gas hydrates have been identified at the crest of this
390 ridge, acoustic flares have so far not been documented (Johnson et al., 2015; Waghorn et al., 2018). We suggest
391 that the N-S trending faults in this region may be impermeable for fluids despite a parallel σ_H , if the stress regime
392 is transpressive. Transpression has been documented at different stages of opening of the Fram Strait (Jokat et al.,
393 2016; Myhre and Eldholm, 1988) and is thus a plausible tectonic mechanism for holding the gas from escaping.
394 Ongoing studies will shed light into the structural evolution of this near-surface system.

395

396 The bathymetry of the southern flank of the Vestnesa Ridge deepens from 1200-1600 m along the crest of the
397 Vestnesa Ridge to ca. 2000 m near the Molloy Transform Fault (Fig. 1). Thus, an additional effect of
398 gravitational stress on near-surface deformation and seepage in the region cannot be ruled out. In particular,
399 although the faults at the steep slope north of the Knipovich Ridge have been suggested to reflect the northward
400 propagation of the Knipovich Ridge rift system (Crane et al., 2001; Vanneste et al., 2005), it is likely that their
401 formation was influenced by gravitational stresses. Small-scale slumps at the slope (Fig 1, 2) could be also
402 evidence of gravitational forcing at the steep southern flank of the Vestnesa Ridge. However, sub-seabed faults

403 on the eastern Vestnesa Ridge dip towards the NE (Fig. 5c), suggesting that gravitational forcing is not
404 necessarily influencing the behaviour of faults and current seepage activity on the eastern Vestnesa Ridge.

405

406 **6.3 Seepage evolution coupled to stress field variations**

407 The seepage systems along the Vestnesa Ridge has been highly dynamic over geological time. Both microbial
408 and thermogenic gas contribute to the gas hydrate and seepage system (Hong et al., 2016;Panieri et al.,
409 2017;Plaza-Faverola et al., 2017;Smith et al., 2014). Reservoir modelling shows that source rock deposited north
410 of the Molloy Transform Fault has potentially started to generate thermogenic gas 6 Ma ago and that migrating
411 fluids reached the Vestnesa Ridge crest at the active seepage site ca. 2 Ma ago (Knies et al., 2018). Seepage has
412 been occurring, episodically, at least since the onset of the Pleistocene glaciations directly through faults, and a
413 deformation typical of gas chimneys (i.e., where periodicity is evidenced by buried pockmarks and authigenic
414 carbonate crusts) seems to have started later (Plaza-Faverola et al., 2015). However, the periodicity of seepage
415 events documented since the Last Glacial Maximum seems to correlate indistinctively with glacials or
416 interglacials (Consolaro et al., 2015;Schneider et al., 2018a;Szybor and Rasmussen, 2017b). One transient event
417 was dated to ca. 17.000 years based on the presence of a ~1000 years old methane-dependent bivalve community
418 possibly sustained by a gas pulse through a fault or chimney (Ambrose et al., 2015). A tectonic control on the
419 evolution of near-surface fluid flow systems and seepage along the Vestnesa Ridge is an explanation that
420 reconciles the numerous cross-disciplinary observations in the area.

421

422 The spatial relation between gas chimneys at the crest of the ridge and fault planes (Fig. 2, 5c) (Bünz et al.,
423 2012;Plaza-Faverola et al., 2015) is intriguing and raises the question whether the faulting was posterior to
424 brecciation (fracturing) of the strata during chimney formation. Gas chimneys form by hydrofracturing generated
425 at a zone of overpressure in a reservoir (e.g., Karstens and Berndt, 2015;Hustoft et al., 2010 and references
426 therein;Davies et al., 2012). From the mechanical point of view the tensile faults at the eastern Vestnesa Ridge
427 would not be a favourable setting for the generation of hydrofracturing and chimney formation right through fault
428 planes as observed in the seismic (Fig. 2, 5c). For gas chimneys to be the youngest features fault segments would
429 have to become tight and permeable at certain periods of times, allowing pore fluid pressure e.g., at the free gas
430 zone beneath the GHSZ to build up (Fig. 5). This is a plausible scenario. The faults may get locally plugged with
431 gas hydrates and authigenic carbonate and activate a self-sealing mechanism similar to that suggested for
432 chimneys at other margins (e.g., Hovland, 2002). A model of gas hydrate-sealed faults and increased free gas
433 zone underneath, has been suggested to explain seismic attenuation and velocities from an ocean bottom seismic

434 experiment over the gas hydrate system north of the Knipovich Ridge (Madrussani et al., 2010). Nevertheless,
435 where gas chimneys do not disturb the seismic response, fault planes are observed to extend near the seafloor
436 (Fig. 5c). This observation suggests that latest faulting periods may have broken through already brecciated
437 regions connecting gas chimneys that were already in place. Both cases are consistent with the fact that acoustic
438 flares and seepage bubbles are restricted to focused weakness zones (Panieri et al., 2017). We suggest that an
439 interaction between pore fluid pressure at the base of the GHSZ and tectonic stress has led to local stress field
440 variations and controlled seepage evolution. Opening of fractures is facilitated if the minimum horizontal stress is
441 smaller than the pore-fluid pressure (p_f), that is, the minimum effective stress is negative ($\sigma_h' = \sigma_h - p_f < 0$) (e.g.,
442 Graults and Baleix, 1994). Secondary permeability may increase by formation of tension fractures near damaged
443 fault zones (Faulkner et al., 2010). Cycles of negative minimum effective stress and subsequent increase in
444 secondary permeability in a tensile stress regime can be achieved particularly easy in the near-surface and would
445 provide an explanation for the development of chimneys coupled to near-surface tectonic deformation. A
446 constant input of thermogenic gas from an Eocene reservoir since at least ca. 2 Ma ago would have contributed to
447 localized pore-fluid pressure increases (Knies et al., 2018).

448

449 Geophysical and paleontological data indicate that there was once more prominent seepage and active chimney
450 development on the western Vestnesa Ridge segment (e.g., Consolaro et al., 2015; Plaza-Faverola et al.,
451 2015; Schneider et al., 2018b). An interaction between pore-fluid pressure and tectonic stress would explain
452 variations in the amount of seepage activity over geological time. Following the same explanation as for the
453 present day seepage, the negative σ_h' condition could have been attained anywhere along the Vestnesa Ridge in
454 the past due to pore fluid pressure increases at the base of the GHSZ or due to favourable stress conditions.
455 During glacial periods, flexural stresses should have been significantly higher than at present day (Lund and
456 Schmidt, 2011). According to recent models of glacial isostasy by the Barents Sea Ice sheet during the last glacial
457 maximum, the Vestnesa Ridge laid in a zone where subsidence could have been of tens of meters (Patton et al.,
458 2016). At other times, before and after glacial maximums, the Vestnesa Ridge was possibly located within the
459 isostatic forebulge.

460

461 In general, it is expected that ~~maximum~~ glacial-induced maximum horizontal stresses (σ_H) would be dominantly
462 oriented parallel to the shelf break (Björn Lund personal communication; Lund et al., 2009), that is, oriented N-S
463 in the area of the Vestnesa Ridge (Fig. 1). Such stress orientation would not favour opening for fluids along pre-
464 existing NW-SE oriented faults associated with seepage activity at present (i.e., N-S oriented faults would be the

465 more vulnerable for opening). It is possible, though, that the repeated waxing and waning of the ice sheet caused
466 a cyclic modulation of the stress field (varying magnitude and orientation) and influenced the dynamics of gas
467 accumulations and favourably oriented faults along the Vestnesa Ridge in the past. Past glacial stresses may
468 provide then an alternative explanation for seepage along the entire Vestnesa Ridge extent at given periods of
469 time (Fig. 6). This explanation is in line with the correlation between seepage and glacial-interglacial events
470 postulated for different continental margins e.g., for chimneys off the mid-Norwegian margin (Plaza-Faverola et
471 al., 2011), the Gulf of Lion (Riboulot et al., 2014), but also along the Vestnesa Ridge (Plaza-Faverola et al.,
472 2015;Schneider et al., 2018b).

473

474 A temporal variation in the stress field along the Vestnesa Ridge is also caused by its location on a constantly
475 growing plate. As the oceanic plate grows, the Vestnesa Ridge moves eastward with respect to the Molloy and
476 Knipovich Ridges, causing a westward shift in the regional stress field on the Vestnesa Ridge (Fig. 7). In future,
477 the eastern Vestnesa Ridge may temporarily move out of the tensile zone, while the western Vestnesa Ridge
478 moves into it (Fig. 7). This suggests that a negative effective stress and subsequent active seepage may reappear
479 and “reactivate” pockmarks to the west of the currently active seepage zone.

480

481 **6.4 Implications for the understanding of near-surface deformation across passive margins**

482 Our study is a first step in the investigation of the effect of regional stress on the dynamics of near-surface fluid
483 flow systems across passive margins. Analytical modelling of spreading at the Molloy and the Knipovich ridges
484 shows that complex stress fields may arise from the interaction of the dynamics at plate boundaries and exert an
485 effect across passive margins. Although the Vestnesa Ridge is a unique case study due to its remarkable
486 proximity to the Arctic mid-ocean ridges, stresses generated by plate tectonic forces are expected to extend for
487 thousands of km (Fejerskov and Lindholm, 2000). Across a single passive margin a range of regional and local
488 factors may result in spatial stress field variations that can explain focusing of gas seepage at specific regions. For
489 instance, the pervasive seepage zone west of Prins Karls Forland (PKF) on the west-Svalbard margin (Fig. 1)
490 could be under a stress regime that has been influenced by glacial rebound at a larger degree than at the Vestnesa
491 Ridge area over geological time. Wallmann et al., (2018) suggested that post glacial uplift lead to gas hydrate
492 dissociation after the Last Glacial Maximum and that such gas continues to sustain seepage off PKF. Previously,
493 several other studies argued for a gas-hydrate control on seepage in this region (e.g., Berndt et al., 2014;Portnov
494 et al., 2016;Westbrook et al., 2009). Since no gas hydrates have been found despite deep drilling (Riedel et al.,
495 2018) the gas hydrate hypotheses remain debatable. The influence of regional stresses on sub-seabed faults

496 suspected to underlay the seepage system (e.g., Mau et al., 2017) and shallow gas reservoirs (Knies et al., 2018)
497 provides an alternative and previously not contemplated explanation for seepage in this area. The interactions
498 between tectonic stress regimes and pore-fluid pressure we propose for explaining seepage evolution along the
499 Vestnesa Ridge may be applicable to seepage systems along other passive margins, in particular along Atlantic
500 passive margins where leakage from hydrocarbon reservoirs is prominent (e.g., the mid-Norwegian margin, the
501 Barents Sea, the North Sea, the north-east Greenland margin, the Mediterranean and even the Scotia plate
502 between Argentina and Antarctica) (e.g., Andreassen et al., 2017; Bünz et al., 2003; Hovland and Sommerville,
503 1985; Riboulot et al., 2014; Somoza et al., 2014; Vis, 2017). The Vestnesa Ridge case study adds a new perspective
504 to the current debate about the inactivity of passive margins (Fejerskov and Lindholm, 2000; Fjeldskaar and
505 Amantov, 2018; Lindholm et al., 2000; Olesen et al., 2013; Stein et al., 1989).

506

507 **7. Conclusions**

508 Analytical modelling of the stress field generated by oblique spreading at the Molloy and Knipovich ridges in the
509 Fram Strait, suggests that spatial variations in the tectonic stress regime along the Vestnesa Ridge are plausible.
510 Thus, mid-ocean ridge spreading may be an important factor controlling faulting and seepage distribution in the
511 region. Other important sources of stress such as bathymetry-gravitational forcing and lithospheric bending,
512 contributing to the actual state of stress off Svalbard, are not considered in the modelling exercise presented here.
513 Hence, we cannot quantitatively assess whether ridge push has a dominant effect on seepage activity. However,
514 provided a certain degree of coupling between crustal and near-surface deformation, it is plausible that stresses
515 from plate spreading may affect the behaviour of Quaternary faults along the Vestnesa Ridge and exert a certain
516 control on seepage. Our study supports a tectonic explanation for the observed seepage pattern in the region. The
517 influence of rifting at the Knipovich Ridge dominantly on the eastern Vestnesa Ridge may be the key for
518 understanding focusing of present day seepage activity along the ridge. The opening of faults and fractures
519 favourably oriented with respect to principal stresses combined with a diminished effective stress in a tensile
520 stress regime facilitates the release of gas from zones of relatively high-pore fluid pressure at the base of the gas
521 hydrate stability zone. Multiple seepage events along the entire extent of the Vestnesa Ridge, may have been
522 induced by additional sources of stress likely associated with glacial isostasy. Future reactivation of currently
523 dormant pockmarks or increase in seepage activity is likely following the gradual westward propagation of the
524 tensile stress zone on the Vestnesa Ridge as the Eurasian plate drifts towards the south-east. Despite the
525 simplifying assumptions by the analytical model approach implemented here, this study provides a first

526 assessment of how important understanding the state of stress is for reconstructing seepage activity along passive
527 margins.

528

529 **8. Outlook**

530 The effect of glacial stresses over the fluid flow system off west-Svalbard will be further tested (at least for the
531 Weichselian period) by implementing Lund et al., models using newly constrained Barents Sea ice-sheet models
532 (e.g., Patton et al., 2016). Additional sources of stress related to topography/bathymetry should be further
533 investigated as well to gain a comprehensive assessment of the effect of the total stress field on near-surface fluid
534 migration in the region.

535

536

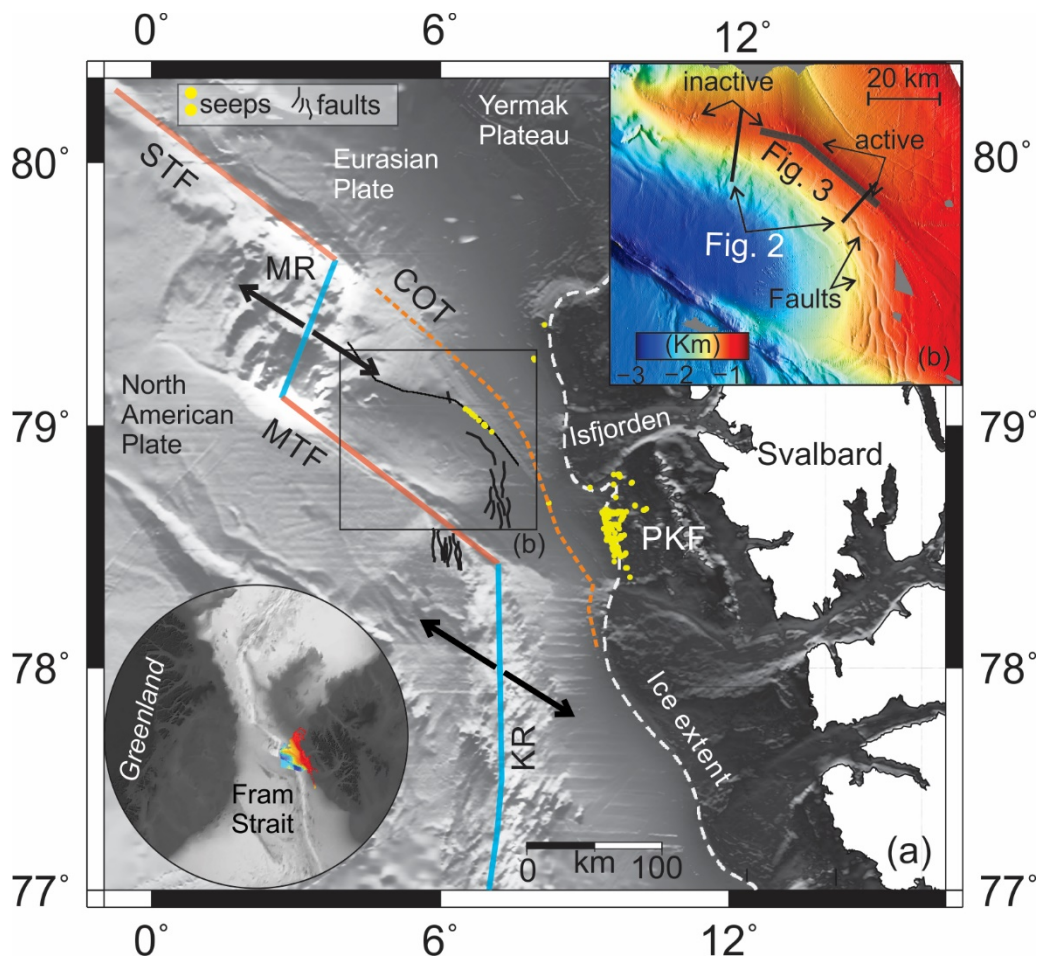
537

538

539

540 **Figures**

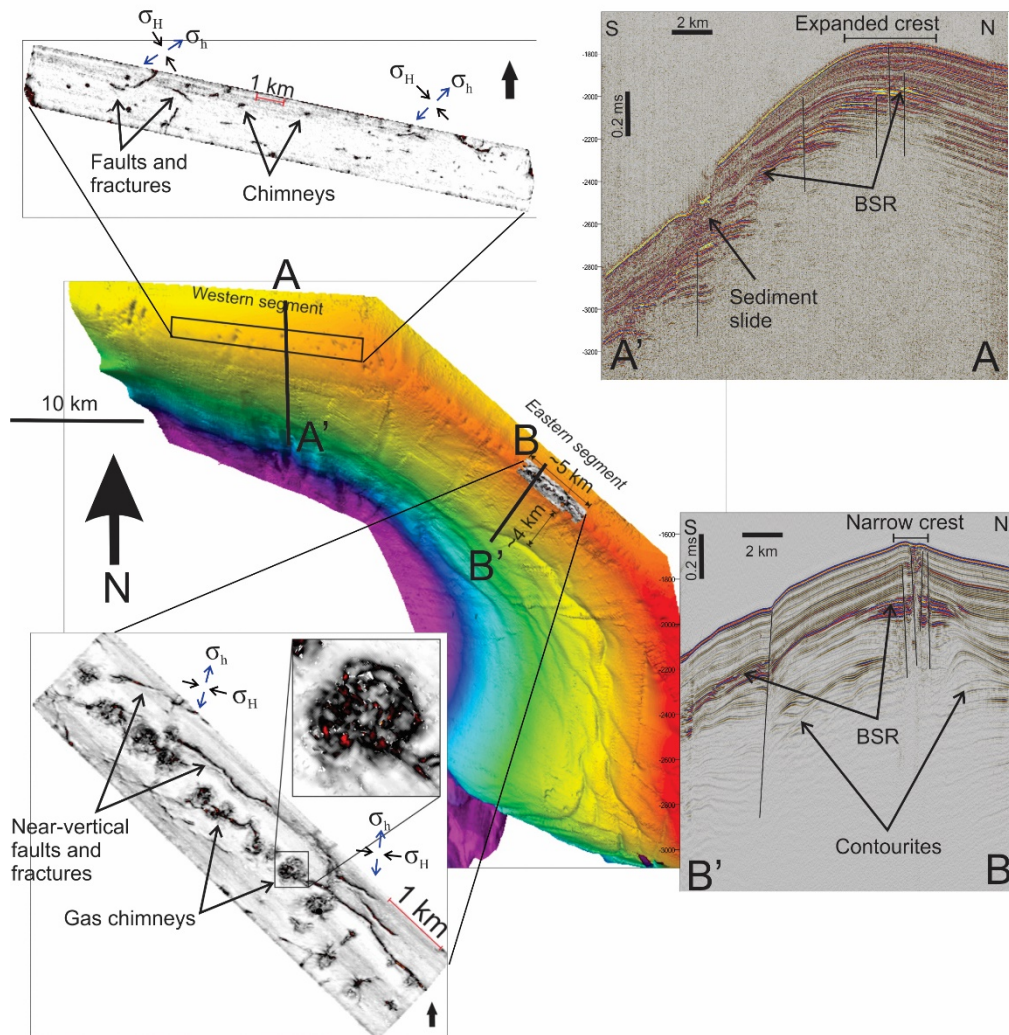
541



542

543 **Figure 1: (a) International Bathymetry Chart of the Arctic Ocean (IBCAO) showing the geometry of mid-**
 544 **ocean ridges offshore the west-Svalbard margin; (b) High resolution bathymetry along the Vestnesa Ridge**
 545 **(UiT, R/V HH multi-beam system). Seafloor pockmarks are observed along the entire ridge but acoustic**
 546 **flares are restricted to the eastern segment; PKF=Prins Karls Forland; STF=Spitsbergen Transform**
 547 **Fault; MR=Molloy Ridge; MTF=Molloy Transform Fault; KR=Knipovich Ridge; COT=Continental-**
 548 **Oceanic Transition (Engen et al., 2008); Ice-Sheet Extent (Patton et al., 2016).**

549

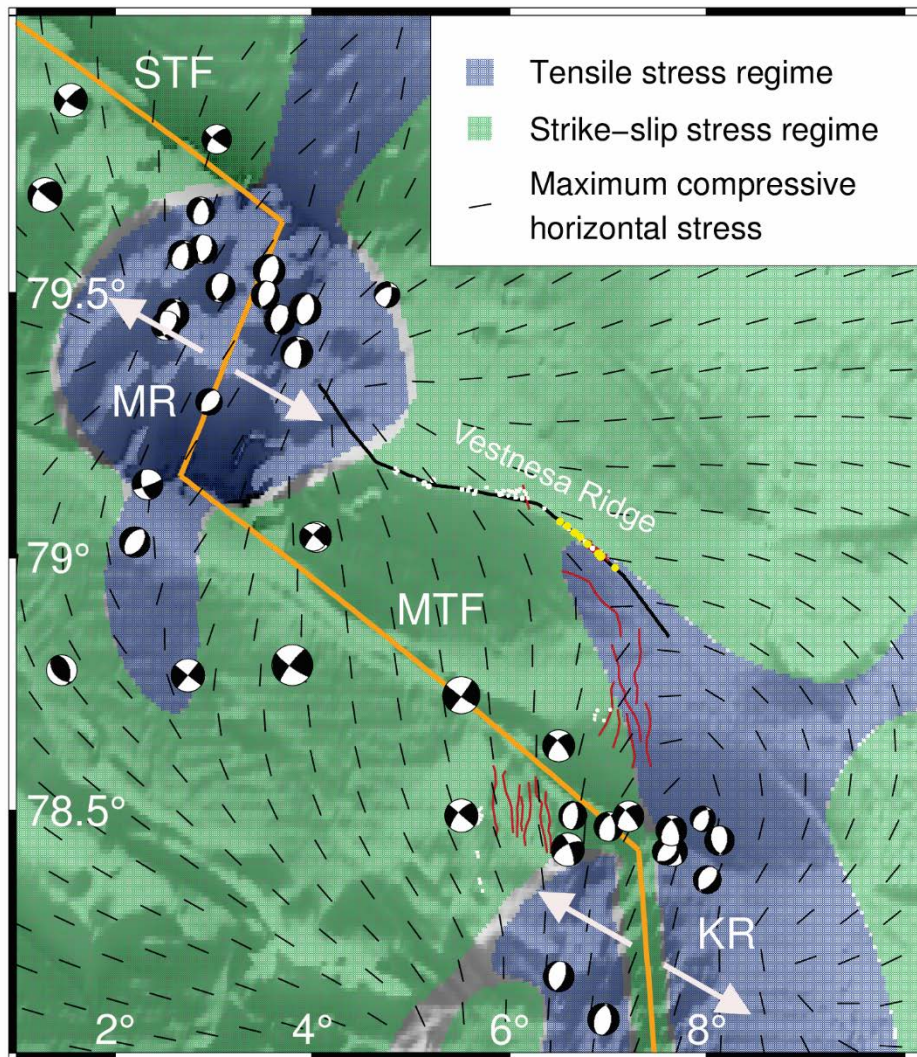


550

551 **Figure 2: Composite figure with bathymetry and variance maps from 3D seismic data along the eastern**
 552 **and the western Vestnesa Ridge segments (modified from Plaza-Faverola et al., 2015). The orientation of**
 553 **maximum compressive horizontal stress (σ_H) and minimum horizontal stress (σ_h) predicted by the model**
 554 **are projected for comparison with the orientation of fault segments. Notice favourable orientation for**
 555 **opening to fluids on the eastern Vestnesa Ridge segment. Two-2D seismic transects (A-A' - Bünz et al.,**
 556 **2012 and B-B' – Johnson et al., 2015) illustrate the morphological difference of the crest of the Vestnesa**
 557 **Ridge (i.e., narrow vs. extended) believed to be determined by bottom current dominated deposition and**
 558 **erosion (Eiken and Hinz, 1993). BSR=bottom simulating reflector.**

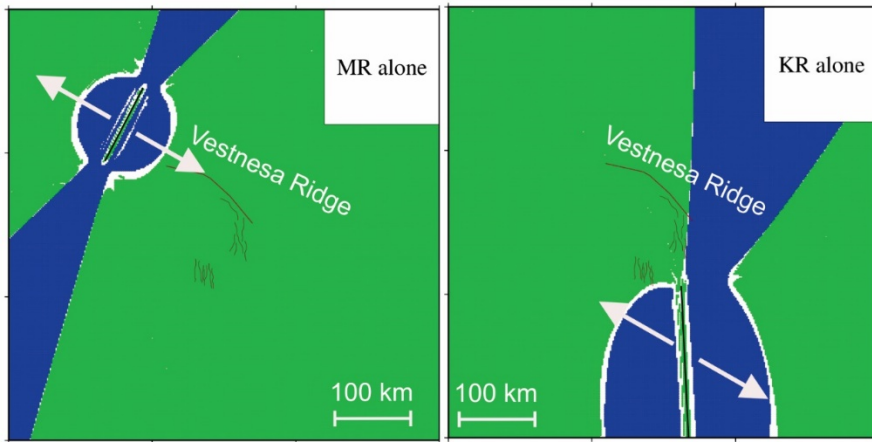
559

560



561

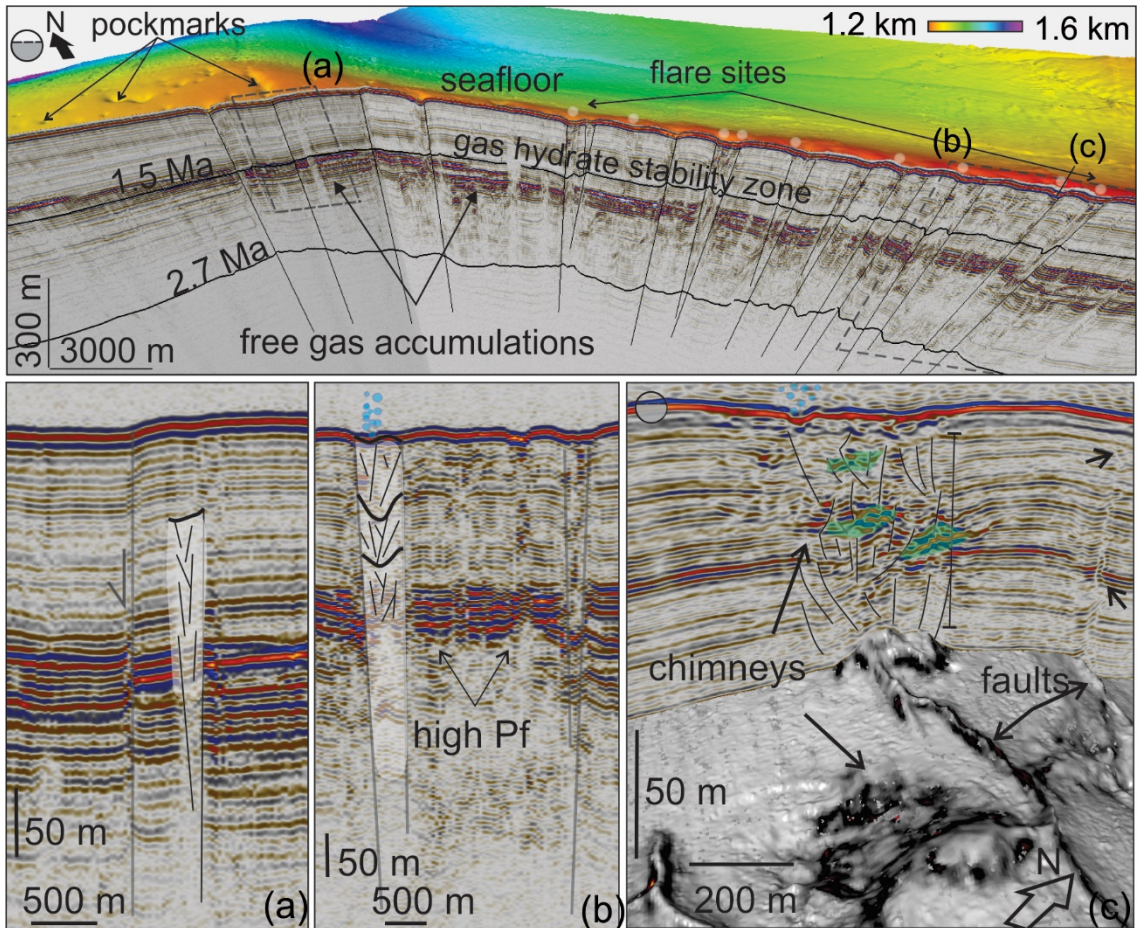
562 **Figure 3: Modelled upper crustal tectonic stress field (blue – tensile and green - strike-slip regime) and**
 563 **stress orientations, due to oblique spreading at the Molloy Ridge (MR) and the Knipovich Ridge (KR). The**
 564 **outline of a seismic line (Plaza-Faverola et al., 2017) is projected as reference for the crest of the Vestnesa**
 565 **Ridge. Red lines are faults, yellow dots seeps and white circles pockmarks where no acoustic flares have**
 566 **been documented. STF=Spitsbergen Transform Fault; MTF=Molloy Transform Fault. The focal**
 567 **mechanisms are from the ISC Online Bulletin (<http://www.isc.ac.uk>).**



568

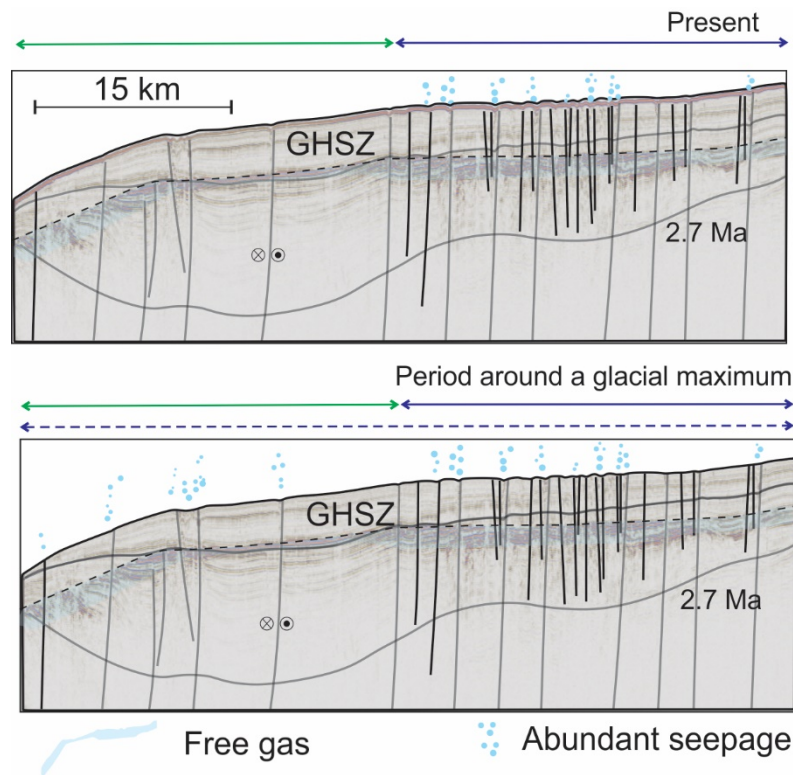
569 **Figure 4: Stress field resulting from model runs with Molloy Ridge and Knipovich Ridge, respectively:**
 570 **tensile stress field (blue); strike-slip stress field (green).**

571



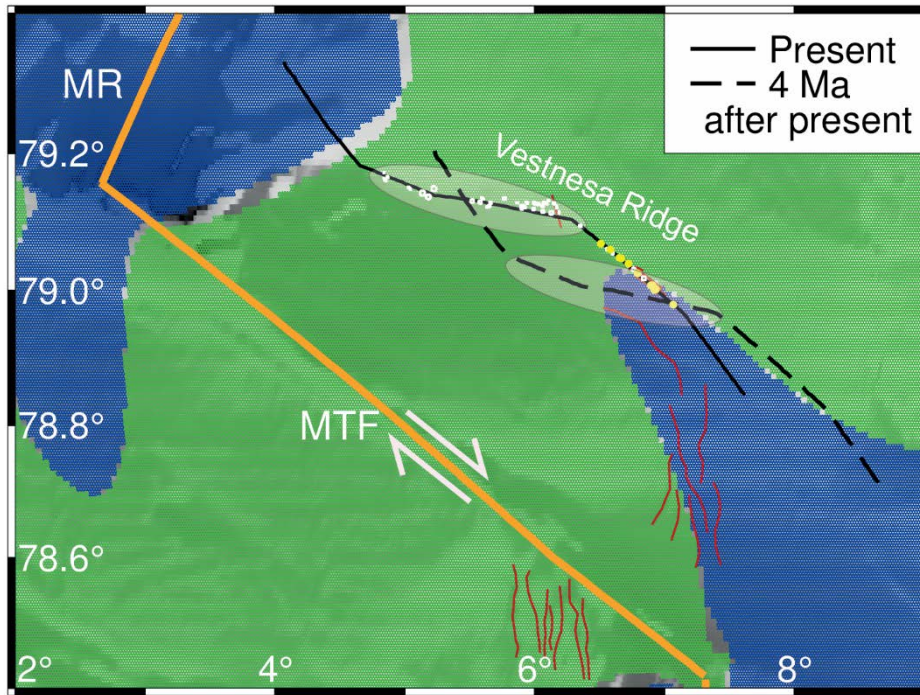
572

573 **Figure 5: Integrated seismic and bathymetry image of the gas hydrate system along the Vestnesa Ridge. (a)**
 574 **Outcropping N-S oriented fault located at the transition from the region where acoustic flares have been**
 575 **documented to the region where no flares have been observed; (b) Gas chimneys with associated acoustic**
 576 **flare and inferred high pore-fluid pressure (Pf) zone at the base of the gas hydrate stability zone;**
 577 **Gas chimney associated with faults and faults extending to near-surface strata without being associated with**
 578 **chimneys. The same variance map in figure 2 is projected at the depth where the map was extracted along**
 579 **a surface interpreted on the 3D seismic volume. Green patches represent interpreted zones of buried**
 580 **authigenic carbonate that can activate a self-sealing mechanism leading to hydrofracturing and chimney**
 581 **development.**
 582



583
 584 **Figure 6: Conceptual model of the evolution of seepage coupled to faulting and spatial variations in the**
 585 **stress regime (tensile=blue; strike-slip=green) along the Vestnesa Ridge, offshore the west-Svalbard**
 586 **margin. At present day, tensile stress from mid-ocean ridge spreading (blue solid line) favours seepage**
 587 **exclusively on the eastern segment of the Vestnesa Ridge. Seepage on the western Vestnesa Ridge and**
 588 **other regions may have been induced repeatedly since the onset of glaciations 2.7 Ma ago (Mattingsdal et**

589 al., 2014), due to tensional flexural stresses (dashed blue line) in the isostatic forebulge around the time of
590 glacial maximums; GHSZ=gas hydrate stability zone. The dashed black line follows the bottom simulating
591 reflector which represents the base of the GHSZ.
592



593
594 **Figure 7: Stress field as in figure 3 showing the location of the Vestnesa Ridge at present and 4 Ma after**
595 **present time, assuming a constant spreading velocity of 7 mm/yr in the direction N125°E. The same line**
596 **outline as in figure 3 is used as reference for the crest of the Vestnesa Ridge. Yellow and white dots**
597 **represent pockmarks with and without documented acoustic flares respectively.**

598

599 **Appendix A**

600 **Model description**

601

602 We use the analytical formulations of Okada (1985) for a finite rectangular dislocation source in elastic
603 homogeneous isotropic half-space (Fig. A.1). The dislocation source can be used to approximate deformation
604 along planar surfaces, such as volcanic dykes (e.g. Wright et al., 2006), sills (e.g. Pedersen and Sigmundsson,
605 2004), faults (e.g. Massonet et al, 1993) and spreading ridges (e.g. Keiding et al., 2009). More than one

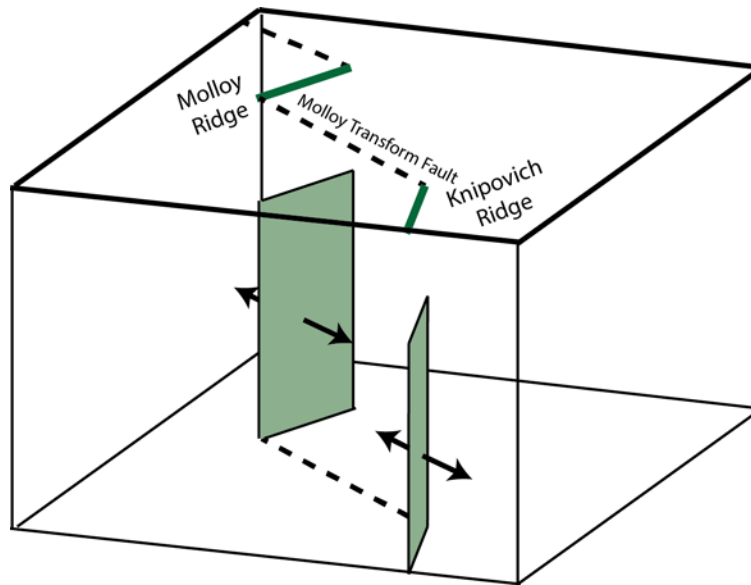
606 dislocation can be combined to obtain more complex geometry of the source or varying deformation along a
607 planar source. The deformation of the source can be defined as either lateral shear (strike-slip for faults), vertical
608 shear (dip-slip at faults) or tensile opening.

609

610 The Okada model assumes flat Earth without inhomogeneities. While the flat-earth assumption is usually
611 adequate for regional studies (e.g. Wolf, 1984), the lateral inhomogeneities can sometimes cause considerable
612 effect on the deformation field (e.g. Okada, 1985). However, the dislocation model is useful as a first
613 approximation to the problem.

614

615 At mid-ocean ridges, deformation is driven by the continuous spreading caused by gravitational stress due to the
616 elevation of the ridges, but also basal drag and possibly slab pull. Deformation occurs continuously in the ductile
617 part of the crust. Meanwhile, elastic strain builds in the upper, brittle part of the crust. To model this setting, the
618 upper boundary of the dislocation source must be located at the depth of the brittle-ductile transition zone. The
619 lower boundary of the source is set to some arbitrary large depth to avoid boundary effects.



620

621 **Fig A.1 Extract of model showing the location of the dislocation sources (light green) for Molloy and**
622 **Knipovich ridges. Note that the model is an infinite half-space, i.e. it has no lateral or lower boundary.**

623

624 The Okada model provides the displacements u_x , u_y , u_z (or velocities if deformation is time-dependent) at defined
625 grid points at the surface and subsurface. It also provides strain (or strain rates) defined as:

626

$$\varepsilon_{ij} = \frac{1}{2}(u_{i,j} + u_{j,i})$$

627

628 The stress field can then be calculated from the predicted strain rates. In homogeneous isotropic media, stress is
629 related to strain as:

630

$$\sigma_{ij} = \lambda \delta_{ij} \varepsilon_{kk} + 2\mu \varepsilon_{ij}$$

631

632 where δ_{ij} is the Kronecker delta, λ is Lamé's first parameter, and μ is the shear modulus. Lamé's first parameter
633 does not have a physical meaning but is related to the shear modulus and Poisson's ratio (ν) as $\lambda = \frac{2\mu\nu}{1-2\nu}$.

634

635 The absolute values of stress are in general difficult to model (e.g. Hergert and Heidbach, 2011), and not possible
636 with our analytical model. However, the model provides us with the orientations and relative magnitude of the
637 stresses. That is, we know the relative magnitudes between the vertical stress (σ_v), maximum horizontal stress
638 (σ_H) and minimum horizontal stress (σ_h). From this, the stress regime can be defined as either tensile ($\sigma_v > \sigma_H >$
639 σ_h), strike-slip ($\sigma_H > \sigma_v > \sigma_h$) or compressive ($\sigma_H > \sigma_h > \sigma_v$).

640

641 **Author contribution**

642 Andreia Plaza-Faverola conceived the paper idea. She is responsible for seismic data processing and
643 interpretation. Marie Keiding did the tectonic modelling. The paper is the result of integrated work between both.

644

645 **ACKNOWLEDGEMENTS**

646 This research is part of the Centre for Arctic Gas Hydrate, Environment and Climate (CAGE) supported by the
647 Research Council of Norway through its Centres of Excellence funding scheme grant No. 223259. Marie Keiding
648 is supported by the NEONOR2 project at the Geological Survey of Norway. Special thanks to Björn Lund, Peter
649 Schmidt, Henry Patton, and Alun Hubbard for their interest in the present project and constructive discussions
650 about isostasy and glacial stresses. We are thankful to various reviewers that have significantly contributed to the
651 improvement of the manuscript. Seismic data is archived at CAGE – Centre for Arctic Gas Hydrate, Environment
652 and Climate, Tromsø, Norway and can be made available by contacting APF. Modelled stresses can be made
653 available by contacting MK.

654

655 **References:**

- 656 Ambrose, W. G., Panieri, G., Schneider, A., Plaza-Faverola, A., Carroll, M. L., Åström, E. K., Locke, W. L., and
657 Carroll, J.: Bivalve shell horizons in seafloor pockmarks of the last glacial-interglacial transition: a thousand years
658 of methane emissions in the Arctic Ocean, *Geochemistry, Geophysics, Geosystems*, 16, 4108-4129, 2015.
- 659 Andreassen, K., Hubbard, A., Winsborrow, M., Patton, H., Vadakkepuliambatta, S., Plaza-Faverola, A.,
660 Gudlaugsson, E., Serov, P., Deryabin, A., and Mattingsdal, R.: Massive blow-out craters formed by hydrate-
661 controlled methane expulsion from the Arctic seafloor, *Science*, 356, 948-953, 2017.
- 662 Árnadóttir, T., Lund, B., Jiang, W., Geirsson, H., Björnsson, H., Einarsson, P., and Sigurdsson, T.: Glacial rebound
663 and plate spreading: results from the first countrywide GPS observations in Iceland, *Geophysical Journal
664 International*, 177, 691-716, 2009.
- 665 Auriac, A., Whitehouse, P., Bentley, M., Patton, H., Lloyd, J., and Hubbard, A.: Glacial isostatic adjustment
666 associated with the Barents Sea ice sheet: a modelling inter-comparison, *Quaternary Science Reviews*, 147, 122-
667 135, 2016.
- 668 Berndt, C., Feseker, T., Treude, T., Krastel, S., Liebetrau, V., Niemann, H., Bertics, V. J., Dumke, I., Dünnbier, K.,
669 and Ferré, B.: Temporal constraints on hydrate-controlled methane seepage off Svalbard, *Science*, 343, 284-287,
670 2014.
- 671 Bünz, S., Mienert, J., and Berndt, C.: Geological controls on the Storegga gas-hydrate system of the mid-
672 Norwegian continental margin, *Earth and Planetary Science Letters*, 209, 291-307, 2003.
- 673 Bünz, S., Polyanov, S., Vadakkepuliambatta, S., Consolaro, C., and Mienert, J.: Active gas venting through
674 hydrate-bearing sediments on the Vestnesa Ridge, offshore W-Svalbard, *Marine geology*, 2012.
- 675 Chand, S., Thorsnes, T., Rise, L., Brunstad, H., Stoddart, D., Bøe, R., Lågstad, P., and Svolsbru, T.: Multiple
676 episodes of fluid flow in the SW Barents Sea (Loppa High) evidenced by gas flares, pockmarks and gas hydrate
677 accumulation, *Earth and Planetary Science Letters*, 331, 305-314, 2012.
- 678 Consolaro, C., Rasmussen, T., Panieri, G., Mienert, J., Bünz, S., and Szttybor, K.: Carbon isotope ($\delta^{13}C$)
679 excursions suggest times of major methane release during the last 14 kyr in Fram Strait, the deep-water
680 gateway to the Arctic, *Climate of the Past*, 11, 669-685, 2015.
- 681 Crane, K., Sundvor, E., Buck, R., and Martinez, F.: Rifting in the northern Norwegian-Greenland Sea: Thermal
682 tests of asymmetric spreading, *Journal of Geophysical Research: Solid Earth*, 96, 14529-14550, 1991.
- 683 Crane, K., Doss, H., Vogt, P., Sundvor, E., Cherkashov, G., Poroshina, I., and Joseph, D.: The role of the
684 Spitsbergen shear zone in determining morphology, segmentation and evolution of the Knipovich Ridge, *Marine
685 geophysical researches*, 22, 153-205, 2001.
- 686 Crutchley, G. J., Berndt, C., Geiger, S., Klaeschen, D., Papenberg, C., Klauke, I., Hornbach, M. J., Bangs, N. L., and
687 Maier, C.: Drivers of focused fluid flow and methane seepage at south Hydrate Ridge, offshore Oregon, USA,
688 *Geology*, 41, 551-554, 2013.
- 689 Davies, R. J., Mathias, S. A., Moss, J., Hustoft, S., and Newport, L.: Hydraulic fractures: How far can they go?,
690 *Marine and petroleum geology*, 37, 1-6, 2012.
- 691 DeMets, C., Gordon, R. G., and Argus, D. F.: Geologically current plate motions, *Geophysical Journal
692 International*, 181, 1-80, 2010.
- 693 DeVore, J. R., and Sawyer, D. E.: Shear strength of siliciclastic sediments from passive and active margins (0–100
694 m below seafloor): insights into seismic strengthening, in: *Submarine Mass Movements and their
695 Consequences*, Springer, 173-180, 2016.

696 Dickens, G. R.: Down the rabbit hole: Toward appropriate discussion of methane release from gas hydrate
697 systems during the Paleocene-Eocene thermal maximum and other past hyperthermal events, *Climate of the*
698 *Past*, 7, 831-846, 2011.

699 Dumke, I., Burwicz, E. B., Berndt, C., Klaeschen, D., Feseker, T., Geissler, W. H., and Sarkar, S.: Gas hydrate
700 distribution and hydrocarbon maturation north of the Knipovich Ridge, western Svalbard margin, *Journal of*
701 *Geophysical Research: Solid Earth*, 121, 1405-1424, 2016.

702 Ehlers, B.-M., and Jokat, W.: Subsidence and crustal roughness of ultra-slow spreading ridges in the northern
703 North Atlantic and the Arctic Ocean, *Geophysical Journal International*, 177, 451-462, 2009.

704 Eiken, O., and Hinz, K.: Contourites in the Fram Strait, *Sedimentary Geology*, 82, 15-32, 1993.

705 Eldholm, O., Faleide, J. I., and Myhre, A. M.: Continent-ocean transition at the western Barents Sea/Svalbard
706 continental margin, *Geology*, 15, 1118-1122, 1987.

707 Engen, Ø., Faleide, J. I., and Dyreng, T. K.: Opening of the Fram Strait gateway: A review of plate tectonic
708 constraints, *Tectonophysics*, 450, 51-69, 2008.

709 Faleide, J., Gudlaugsson, S., Eldholm, O., Myhre, A., and Jackson, H.: Deep seismic transects across the sheared
710 western Barents Sea-Svalbard continental margin, *Tectonophysics*, 189, 73-89, 1991.

711 Faleide, J. I., Solheim, A., Fiedler, A., Hjelstuen, B. O., Andersen, E. S., and Vanneste, K.: Late Cenozoic evolution
712 of the western Barents Sea-Svalbard continental margin, *Global and Planetary Change*, 12, 53-74, 1996.

713 Faulkner, D., Jackson, C., Lunn, R., Schlische, R., Shipton, Z., Wibberley, C., and Withjack, M.: A review of recent
714 developments concerning the structure, mechanics and fluid flow properties of fault zones, *Journal of Structural*
715 *Geology*, 32, 1557-1575, 2010.

716 Fejerskov, M., and Lindholm, C.: Crustal stress in and around Norway: an evaluation of stress-generating
717 mechanisms, Geological Society, London, Special Publications, 167, 451-467, 2000.

718 Fertl, W.: Abnormal Formation Pressures: implications to exploration, drilling and production of oil and gas
719 reservoirs. Development in Petroleum Science 2. Elsevier Scientific Publications Company Amsterdam, 1976.

720 Fjeldskaar, W., and Amantov, A.: Effects of glaciations on sedimentary basins, *Journal of Geodynamics*, 118, 66-
721 81, 2018.

722 Franek, P., Plaza-Faverola, A., Mienert, J., Buenz, S., Ferré, B., and Hubbard, A.: Microseismicity linked to gas
723 migration and leakage on the Western Svalbard Shelf, *Geochemistry, Geophysics, Geosystems*, 18, 4623-4645,
724 2017.

725 Gaina, C., Nikishin, A., and Petrov, E.: Ultraslow spreading, ridge relocation and compressional events in the East
726 Arctic region: A link to the Eurekan orogeny?, *arktos*, 1, 16, 2015.

727 Geersen, J., Scholz, F., Linke, P., Schmidt, M., Lange, D., Behrmann, J. H., Völker, D., and Hensen, C.: Fault zone
728 controlled seafloor methane seepage in the rupture area of the 2010 Maule Earthquake, Central Chile,
729 *Geochemistry, Geophysics, Geosystems*, 17, 4802-4813, 2016.

730 Grauls, D., and Baleix, J.: Role of overpressures and in situ stresses in fault-controlled hydrocarbon migration: A
731 case study, *Marine and Petroleum Geology*, 11, 734-742, 1994.

732 Grunnaleite, I., Fjeldskaar, W., Wilson, J., Faleide, J., and Zweigel, J.: Effect of local variations of vertical and
733 horizontal stresses on the Cenozoic structuring of the mid-Norwegian shelf, *Tectonophysics*, 470, 267-283,
734 2009.

735 Gölke, M., and Coblenz, D.: Origins of the European regional stress field, *Tectonophysics*, 266, 11-24, 1996.

736 Heidbach, O., Rajabi, M., Reiter, K., and Ziegler, M.: World stress map 2016, *Science*, 277, 1956-1962, 2016.

737 Hillis, R. R.: Coupled changes in pore pressure and stress in oil fields and sedimentary basins, *Petroleum*
738 *Geoscience*, 7, 419-425, 2001.

739 Hong, W. L., Sauer, S., Panieri, G., Ambrose, W. G., James, R. H., Plaza-Faverola, A., and Schneider, A.: Removal
740 of methane through hydrological, microbial, and geochemical processes in the shallow sediments of pockmarks
741 along eastern Vestnesa Ridge (Svalbard), *Limnology and Oceanography*, 61, 2016.

742 Hovland, M., and Sommerville, J. H.: Characteristics of two natural gas seepages in the North Sea, *Marine and*
743 *Petroleum Geology*, 2, 319-326, 1985.

744 Hovland, M.: On the self-sealing nature of marine seeps, *Continental Shelf Research*, 22, 2387-2394, 2002.

745 Hunter, S., Goldobin, D., Haywood, A., Ridgwell, A., and Rees, J.: Sensitivity of the global submarine hydrate
746 inventory to scenarios of future climate change, *Earth and Planetary Science Letters*, 367, 105-115, 2013.

747 Hustoft, S., Bünz, S., and Mienert, J.: Three-dimensional seismic analysis of the morphology and spatial
748 distribution of chimneys beneath the Nyegga pockmark field, offshore mid-Norway, *Basin Research*, 22, 465-
749 480, 2010.

750 Hustoft, S., Bunz, S., Mienert, J., Chand, S.: Gas hydrate reservoir and active methane-venting province in
751 sediments on < 20 Ma young oceanic crust in the Fram Strait, offshore NW-Svalbard, *Earth and Planetary*
752 *Science Letters*, 284, 12-24, 10.1016/j.epsl.2009.03.038, 2009.

753 Jakobsson, M., Backman, J., Rudels, B., Nycander, J., Frank, M., Mayer, L., Jokat, W., Sangiorgi, F., O'Regan, M.,
754 and Brinkhuis, H.: The early Miocene onset of a ventilated circulation regime in the Arctic Ocean, *Nature*, 447,
755 986-990, 2007.

756 Jansen, E., Sjøholm, J., Bleil, U., and Erichsen, J.: Neogene and Pleistocene glaciations in the northern
757 hemisphere and late Miocene—Pliocene global ice volume fluctuations: Evidence from the Norwegian Sea, in:
758 *Geological History of the Polar Oceans: Arctic versus Antarctic*, Springer, 677-705, 1990.

759 Jansen, E., and Sjøholm, J.: Reconstruction of glaciation over the past 6 Myr from ice-borne deposits in the
760 Norwegian Sea, *Nature*, 349, 600, 1991.

761 Johnson, J. E., Mienert, J., Plaza-Faverola, A., Vadakkepuliambatta, S., Knies, J., Bünz, S., Andreassen, K., and
762 Ferré, B.: Abiotic methane from ultraslow-spreading ridges can charge Arctic gas hydrates, *Geology*, G36440.
763 36441, 2015.

764 Jokat, W., Lehmann, P., Damaske, D., and Nelson, J. B.: Magnetic signature of North-East Greenland, the Morris
765 Jesup Rise, the Yermak Plateau, the central Fram Strait: constraints for the rift/drift history between Greenland
766 and Svalbard since the Eocene, *Tectonophysics*, 691, 98-109, 2016.

767 Judd, A., and Hovland, M.: *Seabed fluid flow: the impact on geology, biology and the marine environment*,
768 Cambridge University Press, 2009.

769 Jung, N.-H., Han, W. S., Watson, Z., Graham, J. P., and Kim, K.-Y.: Fault-controlled CO₂ leakage from natural
770 reservoirs in the Colorado Plateau, East-Central Utah, *Earth and Planetary Science Letters*, 403, 358-367, 2014.

771 Karstens, J., and Berndt, C.: Seismic chimneys in the Southern Viking Graben—Implications for palaeo fluid
772 migration and overpressure evolution, *Earth and Planetary Science Letters*, 412, 88-100, 2015.

773 Karstens, J., Haflidason, H., Becker, L. W., Berndt, C., Rüpke, L., Planke, S., Liebetrau, V., Schmidt, M., and
774 Mienert, J.: Glacigenic sedimentation pulses triggered post-glacial gas hydrate dissociation, *Nature*
775 *communications*, 9, 635, 2018.

776 Keiding, M., Lund, B., and Árnadóttir, T.: Earthquakes, stress, and strain along an obliquely divergent plate
777 boundary: Reykjanes Peninsula, southwest Iceland, *Journal of Geophysical Research: Solid Earth*, 114, 2009.

778 Knies, J., Matthiessen, J., Vogt, C., Laberg, J. S., Hjelstuen, B. O., Smelror, M., Larsen, E., Andreassen, K., Eidvin,
779 T., and Vorren, T. O.: The Plio-Pleistocene glaciation of the Barents Sea–Svalbard region: a new model based on
780 revised chronostratigraphy, *Quaternary Science Reviews*, 28, 812-829,
781 <http://dx.doi.org/10.1016/j.quascirev.2008.12.002>, 2009.

782 Knies, J., Daszinnies, M., Plaza-Faverola, A., Chand, S., Sylta, Ø., Bünz, S., Johnson, J. E., Mattingsdal, R., and
783 Mienert, J.: Modelling persistent methane seepage offshore western Svalbard since early Pleistocene, *Marine
784 and Petroleum Geology*, 91, 800-811, 2018.

785 Lindholm, C. D., Bungum, H., Hicks, E., and Villagran, M.: Crustal stress and tectonics in Norwegian regions
786 determined from earthquake focal mechanisms, Geological Society, London, Special Publications, 167, 429-439,
787 2000.

788 Lund, B., and Townend, J.: Calculating horizontal stress orientations with full or partial knowledge of the
789 tectonic stress tensor, *Geophysical Journal International*, 170, 1328-1335, 2007.

790 Lund, B., Schmidt, P., and Hieronymus, C.: Stress evolution and fault stability during the Weichselian glacial
791 cycle, Swedish Nuclear Fuel and Waste Management Co, Stockholm, Sweden, Tech. Rep. TR-09-15, 2009.

792 Lund, B., and Schmidt, P.: Stress evolution and fault stability at Olkiluoto during the Weichselian glaciation,
793 Report for Posiva Oy, 2011.

794 Madrussani, G., Rossi, G., and Camerlenghi, A.: Gas hydrates, free gas distribution and fault pattern on the west
795 Svalbard continental margin, *Geophysical Journal International*, 180, 666-684, 2010.

796 Mattingsdal, R., Knies, J., Andreassen, K., Fabian, K., Husum, K., Grøsfjeld, K., and De Schepper, S.: A new 6 Myr
797 stratigraphic framework for the Atlantic–Arctic Gateway, *Quaternary Science Reviews*, 92, 170-178, 2014.

798 Mau, S., Römer, M., Torres, M. E., Bussmann, I., Pape, T., Damm, E., Geprägs, P., Wintersteller, P., Hsu, C.-W.,
799 and Loher, M.: Widespread methane seepage along the continental margin off Svalbard—from Bjørnøya to
800 Kongsfjorden, *Scientific reports*, 7, 42997, 2017.

801 Minshull, T., and White, R.: Sediment compaction and fluid migration in the Makran accretionary prism, *Journal
802 of Geophysical Research: Solid Earth*, 94, 7387-7402, 1989.

803 Moore, J. C., and Vrolijk, P.: Fluids in accretionary prisms, *Reviews of Geophysics*, 30, 113-135, 1992.

804 Morgan, W. J.: 13. Hotspot tracks and the opening of the Atlantic and Indian Oceans, *The oceanic lithosphere*, 7,
805 443, 1981.

806 Myhre, A. M., and Eldholm, O.: The western Svalbard margin (74–80 N), *Marine and Petroleum Geology*, 5, 134-
807 156, 1988.

808 Naliboff, J., Lithgow-Bertelloni, C., Ruff, L., and de Koker, N.: The effects of lithospheric thickness and density
809 structure on Earth's stress field, *Geophysical Journal International*, 188, 1-17, 2012.

810 Nasuti, A., and Olesen, O.: Chapter 4: Magnetic data. In: Hopper J.R., Funck T., Stoker T., Arting U., Peron-
811 Pinvidic G., Doornebal H. & Gaina C. (eds) *Tectonostratigraphic Atlas of the North-East Atlantic Region*.
812 Geological Survey of Denmark and Greenland (GEUS), Copenhagen, Denmark, 41–51. , 2014.

813 Okada, Y.: Surface deformation due to shear and tensile faults in a half-space, *Bulletin of the seismological
814 society of America*, 75, 1135-1154, 1985.

815 Olesen, O., Bungum, H., Dehls, J., Lindholm, C., Pascal, C., and Roberts, D.: Neotectonics, seismicity and
816 contemporary stress field in Norway—mechanisms and implications, *Quaternary Geology of Norway*, Geological
817 Survey of Norway Special Publication, 13, 145-174, 2013.

818 Panieri, G., Bünz, S., Fornari, D. J., Escartin, J., Serov, P., Jansson, P., Torres, M. E., Johnson, J. E., Hong, W., and
819 Sauer, S.: An integrated view of the methane system in the pockmarks at Vestnesa Ridge, 79° N, *Marine
820 Geology*, 390, 282-300, 2017.

821 Patton, H., Hubbard, A., Andreassen, K., Winsborrow, M., and Stroeven, A. P.: The build-up, configuration, and
822 dynamical sensitivity of the Eurasian ice-sheet complex to Late Weichselian climatic and oceanic forcing,
823 *Quaternary Science Reviews*, 153, 97-121, 2016.

824 Petersen, C. J., Bünz, S., Hustoft, S., Mienert, J., and Klaeschen, D.: High-resolution P-Cable 3D seismic imaging
825 of gas chimney structures in gas hydrated sediments of an Arctic sediment drift, *Marine and Petroleum*
826 *Geology*, doi: 10.1016/j.marpetgeo.2010.06.006, 1-14, DOI: 10.1016/j.marpetgeo.2010.06.006, 2010.

827 Planke, S., Eriksen, F. N., Berndt, C., Mienert, J., and Masson, D.: P-Cable high-resolution seismic, *Oceanography*,
828 22, 85, 2009.

829 Plaza-Faverola, A., Bünz, S., and Mienert, J.: Repeated fluid expulsion through sub-seabed chimneys offshore
830 Norway in response to glacial cycles, *Earth and Planetary Science Letters*, 305, 297-308,
831 10.1016/j.epsl.2011.03.001, 2011.

832 Plaza-Faverola, A., Bünz, S., Johnson, J. E., Chand, S., Knies, J., Mienert, J., and Franek, P.: Role of tectonic stress
833 in seepage evolution along the gas hydrate-charged Vestnesa Ridge, Fram Strait, *Geophys. Res. Lett.*, 42, 733-
834 742, 2015.

835 Plaza-Faverola, A., Henrys, S., Pecher, I., Wallace, L., and Klaeschen, D.: Splay fault branching from the Hikurangi
836 subduction shear zone: Implications for slow slip and fluid flow, *Geochemistry, Geophysics, Geosystems*, 17,
837 5009-5023, 2016.

838 Plaza-Faverola, A., Vadakkepuliymbatta, S., Hong, W. L., Mienert, J., Bünz, S., Chand, S., and Greinert, J.:
839 Bottom-simulating reflector dynamics at Arctic thermogenic gas provinces: an example from Vestnesa Ridge,
840 offshore west-Svalbard, *Journal of Geophysical Research: Solid Earth*, 2017.

841 Portnov, A., Vadakkepuliymbatta, S., Mienert, J., and Hubbard, A.: Ice-sheet-driven methane storage and
842 release in the Arctic, *Nature communications*, 7, 10314, 2016.

843 Riboulot, V., Thomas, Y., Berné, S., Jouet, G., and Cattaneo, A.: Control of Quaternary sea-level changes on gas
844 seeps, *Geophys. Res. Lett.*, 41, 4970-4977, 2014.

845 Riedel, M., Wallmann, K., Berndt, C., Pape, T., Freudenthal, T., Bergenthal, M., Bünz, S., and Bohrmann, G.: In
846 situ temperature measurements at the Svalbard Continental Margin: Implications for gas hydrate dynamics,
847 *Geochemistry, Geophysics, Geosystems*, 19, 1165-1177, 2018.

848 Roy, S., Senger, K., Braathen, A., Noormets, R., Hovland, M., and Olausen, S.: Fluid migration pathways to
849 seafloor seepage in inner Isfjorden and Adventfjorden, Svalbard, *Geological controls on fluid flow and seepage*
850 *in western Svalbard fjords, Norway. An integrated marine acoustic study*, 2014.

851 Salomatin, A., and Yusupov, V.: Acoustic investigations of gas “flares” in the Sea of Okhotsk, *Oceanology*, 51,
852 857, 2011.

853 Salomon, E., Koehn, D., Passchier, C., Hackspacher, P. C., and Glasmacher, U. A.: Contrasting stress fields on
854 correlating margins of the South Atlantic, *Gondwana research*, 28, 1152-1167, 2015.

855 Schiffer, C., Tegner, C., Schaeffer, A. J., Pease, V., and Nielsen, S. B.: High Arctic geopotential stress field and
856 implications for geodynamic evolution, *Geological Society, London, Special Publications*, 460, 441-465, 2018.

857 Schneider, A., Panieri, G., Lepland, A., Consolaro, C., Crémière, A., Forwick, M., Johnson, J., Plaza-Faverola, A.,
858 Sauer, S., and Knies, J.: Methane seepage at Vestnesa Ridge (NW Svalbard) since the Last Glacial Maximum,
859 *Quaternary Science Reviews*, 193, 98-117, 2018a.

860 Schneider, A., Panieri, G., Lepland, A., Consolaro, C., Crémière, A., Forwick, M., Johnson, J. E., Plaza-Faverola, A.,
861 Sauer, S., and Knies, J.: Methane seepage at Vestnesa Ridge (NW Svalbard) since the Last Glacial Maximum,
862 *Quaternary Science Reviews*, 193, 98-117, <https://doi.org/10.1016/j.quascirev.2018.06.006>, 2018b.

863 Sibson, R. H.: Crustal stress, faulting and fluid flow, *Geological Society, London, Special Publications*, 78, 69-84,
864 1994.

865 Skarke, A., Ruppel, C., Kodis, M., Brothers, D., and Lobecker, E.: Widespread methane leakage from the sea floor
866 on the northern US Atlantic margin, *Nature Geoscience*, 7, 657-661, 2014.

867 Smith, A. J., Mienert, J., Bünz, S., and Greinert, J.: Thermogenic methane injection via bubble transport into the
868 upper Arctic Ocean from the hydrate-charged Vestnesa Ridge, Svalbard, *Geochemistry, Geophysics,*
869 *Geosystems*, 2014.

870 Smith, S. B., Denzil Taylor: Deep-sea sediment compression curves: Some controlling factors, spurious
871 overconsolidation, predictions, and geophysical reproduction, *Marine Georesources and Geotechnology*, 17, 65-
872 81, 1999.

873 Somoza, L., León, R., Medialdea, T., Pérez, L. F., González, F. J., and Maldonado, A.: Seafloor mounds, craters
874 and depressions linked to seismic chimneys breaching fossilized diagenetic bottom simulating reflectors in the
875 central and southern Scotia Sea, Antarctica, *Global and Planetary Change*, 123, 359-373, 2014.

876 Steffen, H., Kaufmann, G., and Wu, P.: Three-dimensional finite-element modeling of the glacial isostatic
877 adjustment in Fennoscandia, *Earth and Planetary Science Letters*, 250, 358-375, 2006.

878 Stein, S., Cloetingh, S., Sleep, N. H., and Wortel, R.: Passive margin earthquakes, stresses and rheology, in:
879 *Earthquakes at North-Atlantic Passive Margins: Neotectonics and Postglacial Rebound*, Springer, 231-259, 1989.

880 Svensen, H., Planke, S., Malthe-Sørensen, A., Jamtveit, B., Myklebust, R., Eidem, T. R., and Rey, S. S.: Release of
881 methane from a volcanic basin as a mechanism for initial Eocene global warming, *Nature*, 429, 542-545, 2004.

882 Szybor, K., and Rasmussen, T. L.: Diagenetic disturbances of marine sedimentary records from
883 methane-influenced environments in the Fram Strait as indications of variation in seep intensity during the last
884 35 000 years, *Boreas*, 46, 212-228, 2017a.

885 Szybor, K., and Rasmussen, T. L.: Late glacial and deglacial palaeoceanographic changes at Vestnesa Ridge,
886 Fram Strait: Methane seep versus non-seep environments, *Palaeogeography, Palaeoclimatology, Palaeoecology*,
887 476, 77-89, 2017b.

888 Turcotte, D., Ahern, J., and Bird, J.: The state of stress at continental margins, *Tectonophysics*, 42, 1-28, 1977.

889 Turcotte, D. L., and Schubert, G.: *Geodynamics*, Cambridge University Press, New York, 2002.

890 Urlaub, M., Talling, P. J., Zervos, A., and Masson, D.: What causes large submarine landslides on low gradient (<
891 2°) continental slopes with slow (~ 0.15 m/kyr) sediment accumulation?, *Journal of Geophysical Research: Solid*
892 *Earth*, 120, 6722-6739, 2015.

893 Vanneste, M., Guidard, S., and Mienert, J.: Arctic gas hydrate provinces along the western Svalbard continental
894 margin, *Norwegian Petroleum Society Special Publications*, 12, 271-284, 2005.

895 Vis, G.-J.: *Geology and seepage in the NE Atlantic region*, Geological Society, London, Special Publications, 447,
896 SP447. 416, 2017.

897 Vogt, P. R., Crane, K., Sundvor, E., Max, M. D., and Pfirman, S. L.: Methane-generated (?) pockmarks on young,
898 thickly sedimented oceanic crust in the Arctic: Vestnesa ridge, Fram strait, *Geology*, 22, 255-258, 1994.

899 Waghorn, K. A., Bünz, S., Plaza-Faverola, A., and Johnson, J. E.: 3D Seismic Investigation of a Gas Hydrate and
900 Fluid Flow System on an Active Mid-Ocean Ridge; Svyatogor Ridge, Fram Strait, *Geochemistry, Geophysics,*
901 *Geosystems*, 2018.

902 Wallmann, K., Riedel, M., Hong, W., Patton, H., Hubbard, A., Pape, T., Hsu, C., Schmidt, C., Johnson, J., and
903 Torres, M.: Gas hydrate dissociation off Svalbard induced by isostatic rebound rather than global warming,
904 *Nature communications*, 9, 83, 2018.

905 Westbrook, G. K., Thatcher, K. E., Rohling, E. J., Piotrowski, A. M., Palike, H., Osborne, A. H., Nisbet, E. G.,
906 Minshull, T. A., Lanoiselle, M., James, R. H., Huhnerbach, V., Green, D., Fisher, R. E., Crocker, A. J., Chabert, A.,
907 Bolton, C., Beszczynska-Moller, A., Berndt, C., and Aquilina, A.: Escape of methane gas from the seabed along
908 the West Spitsbergen continental margin, *Geophys. Res. Lett.*, 36, 5, L1560810.1029/2009gl039191, 2009.

909 Zoback, M. D., and Zoback, M. L.: 34 State of stress in the Earth's lithosphere, *International Geophysics*, 81, 559-
910 XII, 2002.
911